Chapter 11: Syngas-based Pathways for SAF: Fischer-Tropsch Synthesis

Cherie Hsu[1] and Moritz Wolf[1,2]*.

[1]Karlsruhe Institute of Technology (KIT), Institute of Catalysis Research and Technology (IKFT), Hermann-von-Helmholtz-Platz 1, 76344 Eggenstein-Leopoldshafen, Germany

[2]Karlsruhe Institute of Technology (KIT), Engler-Bunte-Institut (EBI), Engler-Bunte-Ring 3, 76131 Karlsruhe, Germany

*corresponding email address: moritz.wolf@kit.edu

ABSTRACT/WEB SUMMARY

"**Syngas-based Pathways for SAF: Fischer-Tropsch Synthesis** – *The production of sustainable aviation fuel (SAF) using syngas and Fischer-Tropsch synthesis (FTS) is explored in this chapter, with a particular emphasis on sustainable syngas production pathways. Using gasification of biomass and the Fischer-Tropsch process for the generation of SAF provides a biomass-to-liquid (BTL) route, while power-based approaches for the generation of syngas together with FTS represent the power-to-liquid (PTL) route. A thorough grasp of the historical evolutions, technical issues, recent milestones and long-term prospects is provided for the FTS.*"

KEYWORDS

CO hydrogenation; Fischer-Tropsch catalyst; Synthesis gas production; Synthetic fuels; Synthetic kerosene

11.1 Introduction

In the era of energy transition with the goal to overcome the impact to climate change, sustainable aviation fuel (SAF) poses as a key potential solution for defossilisation of the hard-to-abate aviation sector. SAF production via Fischer-Tropsch synthesis (FTS) has shown promise as a viable pathway based on the years of research and development already done in Fischer-Tropsch (FT) process[1]. The FT process is a series of chemical reactions that produces and transforms synthesis gas (syngas), a mixture of carbon monoxide (CO) and hydrogen (H_2), into hydrocarbons and water. The wide range of liquid hydrocarbon products is converted in a subsequent step to maximise the yield of the desired fraction in a final product make-up. This high degree of flexibility makes the FT process highly adjustable. Nevertheless, the actual FTS is the crucial step for maximum overall yield of SAF, which is produced directly and additionally targeted in the down-stream processing of long-chain hydrocarbons. The FTS requires a metal-based catalyst, such as any group VIII transition metal, to support the reaction at temperature around 150 to 350 °C and pressure of 20 to 35 bars. Iron (Fe) and cobalt (Co) are the industrially viable FT catalysts[2]. Advancements in catalysis research have made the syngas pathway of producing SAF more efficient and adaptable[1].

Production of SAF is one of the energy transition solutions to fulfil the environmental targets of climate neutrality in the European Union (EU) by 2050 provided by the European Green Deal from the EU Emission Trading System (ETS) and the global measures known as the Carbon Offsetting and Reduction Scheme for International Aviation (CORSIA) from the International Civil Aviation Organisation (ICAO)[3]. The Department of Energy (DoE) in the United States of America (USA) targets an annual production of 3 billion gallons of SAF by

2030 and 35 billion gallons by 2050[4]. Furthermore, recent research innovation of integrating carbon dioxide (CO_2) into the synthesis process would open up new potential for reducing carbon emissions. Currently, FT processes based on fossil feedstock is an important process being used in the coal-to-liquid (CTL) and gas-to-liquid (GTL) commercial process plants, such as Secunda CTL plant by Sasol in South Africa and Pearl GTL plant by Shell in Qatar[5].

Interest in the FT process flared up numerous times in the last century. Based on the knowledge gained by Franz Fischer and Hans Tropsch during extensive research studies on the CO hydrogenation over finely dispersed cobalt-, iron-, and nickel-based catalysts in the 1920s at the Kaiser Wilhelm Institute for Coal Research (now: Max-Planck-Institut für Kohlenforschung) in Mülheim an der Ruhr[6, 7], Ruhrchemie acquired the license and commissioned the first plants of industrial scale in Germany from 1934-1948[8-10]. These early stages of the industrialisation of the FT process were rather driven by geopolitical reasons than commercial aspects as the FT-derived fuels provided an important strategical independence from trade embargos before and during World War II. For example, the Brabag Schwarzheide FT plant in Lusatia had a production capacity of 1,500 barrels per day (bpd)[9, 10]. Syngas was generated via gasification of coal representing the first indirect CTL process[8, 10, 11]. Aside from the plants in Germany, licensed plants were erected in France, Manchuria (today: People's Republic of China, PRC), and Japan[12]. However, all plants were decommissioned after the war as the FT process could not compete with the low crude oil price[9, 10].

In the 1950s, the readily available enormous coal reserves in South Africa in combination with forecasted crude oil price hikes revived the industrial FT process. The government-funded South African Coal, Oil and Gas Corporation (Sasol) was founded in 1950 and a first CTL plant with a capacity of 2,500 bpd was commissioned in Sasolburg in 1955[9, 11, 12]. First major crude oil price hikes (see Figure 11.1) due to wars and conflicts in the Middle-East, as well as the Arab Oil Embargo increased the commercial viability drastically. Such spikes together with an increasing political isolation during apartheid, which involved economic sanctions like trade

embargos, provoked the construction of additional CTL plants in the early 80s. Secunda I and II represent the first commercially viable FT plants with a combined capacity of 160,000 bpd[12].

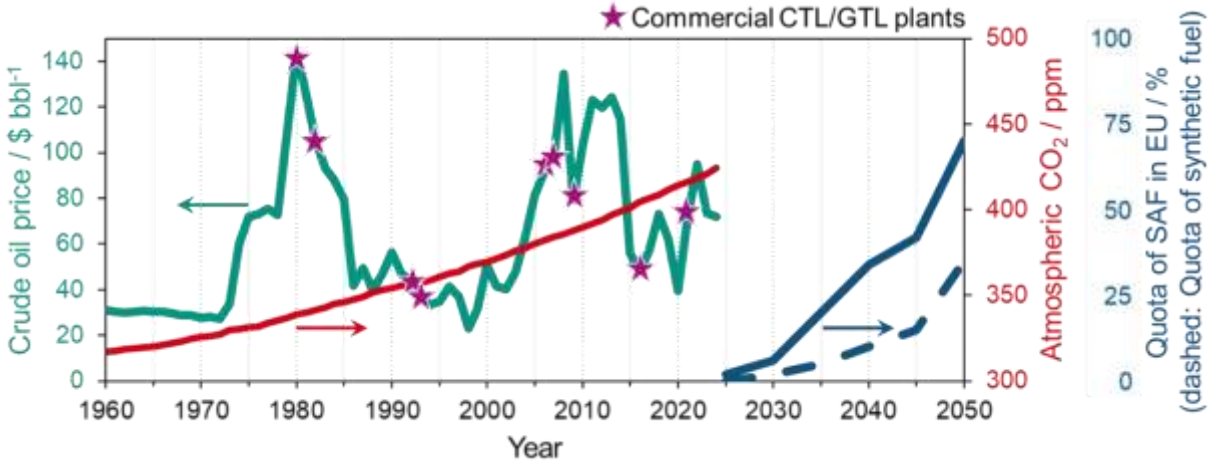

Figure 11.1 *Historical inflation adjusted crude oil price[13] with years of commissioning of commercial CTL and GTL FT plants together with the historical atmospheric concentration of CO_2[14, 15] and quota for SAF at European airports according to the ReFuelEU[3] regulation of the EU as new driving forces of the FT technology.*

Steam reforming of natural gas is the most economical way to produce syngas. Consequently, the GTL pathway has a significantly lower break-even oil price and also decreases the carbon footprint by approx. 50% when compared to the CTL process[16]. Therefore, almost exclusively GTL facilities were commissioned on large scale in the recent decades: Mossgas (now: Petroleum, Oil and Gas Corporation of South Africa (PetroSA)) in Mossel Bay (Republic of South Africa (RSA), 36,000 bpd, in operation until 2020), Shell in Bintulu (Malaysia, 14,500 bpd) and Ras Laffan (Qatar, 140,000 bpd), Sasol in joint venture with Qatar Petroleum in Ras Laffan (Qatar, 34,000 bpd), Sasol in joint venture with Chevron in Escravos (Nigeria, 33,200 bpd), as well as Sasol and Petronas in joint venture with Uzbekneftegaz in the Kashkadarya region (Uzbekistan, 37,650 bpd)[9-11, 17]. The USA and PRC have the highest energy demand of all countries and they own enormous coal reserves[18-20]. Hence, both countries have a great potential for CTL plants[17, 19, 20] as demonstrated by the recent commissioning of the largest single CTL plant in the world in the Ningxia region (PRC,

100,000 bpd)[21, 22]. However, the challenges of commissioning and viable operation of FT plants from an economic point of view are strongly linked to the crude oil price.

More recently, the drastically pronounced effects of climate change represent another driving force for the development of FT processes leading to a large number of companies mostly focussing on the production of SAF and shipping fuel, two hard-to-abate transportation sectors, such as Velocys and Topsoe[23]. In response to the continuously increasing concentration of CO_2 in the atmosphere and in an attempt to reach the Paris agreement of limiting global warming to 1.5 °C[3], the EU decided on ambitious target shares of SAF at EU airports (see Figure 11.1). This legislative driving force for an accelerated development of SAF represents a new approach as a commercial viability still represents the major challenge. In the regulation, a stepwise increase of the share from 2% in 2025 up to 70% in 2050 is targeted with relative share of SAF of 35% to enable climate neutrality by 2050 at the latest[3]. This corresponds to a demand of approx. 20 Mt of synthetic aviation fuels in 2050, which has to be covered via FT processes or related syngas-based routes, such as methanol-to-jet fuel (MTJ).

The production of synthetic fuels and chemicals via the biomass-to-liquid (BTL) is fully based on renewable feedstock[17, 24, 25], but the break-even oil price lies above the one for the CTL process[16]. Here, the smaller scale of the FT process due to limited local feedstock availability when compared to fossil resources becomes particular challenging and typically lowers the efficiency. Similarly, the power-to-liquid (PTL) route is not yet competitive, but is more susceptible to regulatory measures due to the dominating role of the electricity price as major cost driver aside from the source of CO_2. The feedstock potential and production scales are superior when compared to alternative production routes for SAF. Ramp up of existing technologies for harvesting renewable energy, such as photovoltaics and wind parks, may provide sufficient electricity to drive the various energy demanding processes. In particular the renewable potential of solar irradiation is more than a magnitude above the one for biomass conversion, while wind energy has a more than 10 times increased potential[26]. Economic and regulatory incentives and global partnerships are required to tap this infinite potential.

In this chapter, sustainable production routes for syngas and its conversion in the FT process are presented. The most advanced technologies for sustainable syngas production are discussed in detail, namely gasification of biomass, reforming of biogas and the reverse water-gas shift reaction (RWGS). These technologies are compared with the state-of-the-art solutions and several alternative pathways experiencing a rapid technological development are described as well. In the second part of this chapter, a detailed description of the FT process with a particular focus on the most important levers for maximising the production of SAF are presented. Here, the synthesis of long-chain hydrocarbons is targeted, which can be achieved by, amongst other parameters, the optimisation and adaption of the FT catalysts. Lastly, selected milestones for the production and application of SAF from FT processes are discussed alongside an outlook for the overall potential of the syngas-based FT route.

11.2 Production of Syngas

11. 2. 1. Overview of State-of-the-Art and (Future) Sustainable Alternatives

The majority of the energy and feedstock demand in the chemical industry is met by fossil fuels, which is also the case in state-of-the-art syngas production. The actual process of choice for each individual chemical site is a feedstock-based decision. The first FT processes via the CTL route in Germany using cobalt-based catalysts were based on coal gasification followed by water-gas shift (WGS) reaction to meet the required ratio of H_2:CO of ~2:1 in the syngas. The first Sasol CTL plants are based on WGS active iron-based catalysts rendering a separate WGS stage for adjusting the syngas composition obsolete. Since the 1990s, GTL routes were commercialised as a consequence of the increase crude oil price following the oil crisis in the 1970s. Various process options have been established for the conversion of natural gas to syngas, namely steam reforming, autothermal reforming, and partial oxidation. These reforming processes typically provide a favourable H_2:CO ratio larger than 2:1 (see Figure 11.2).

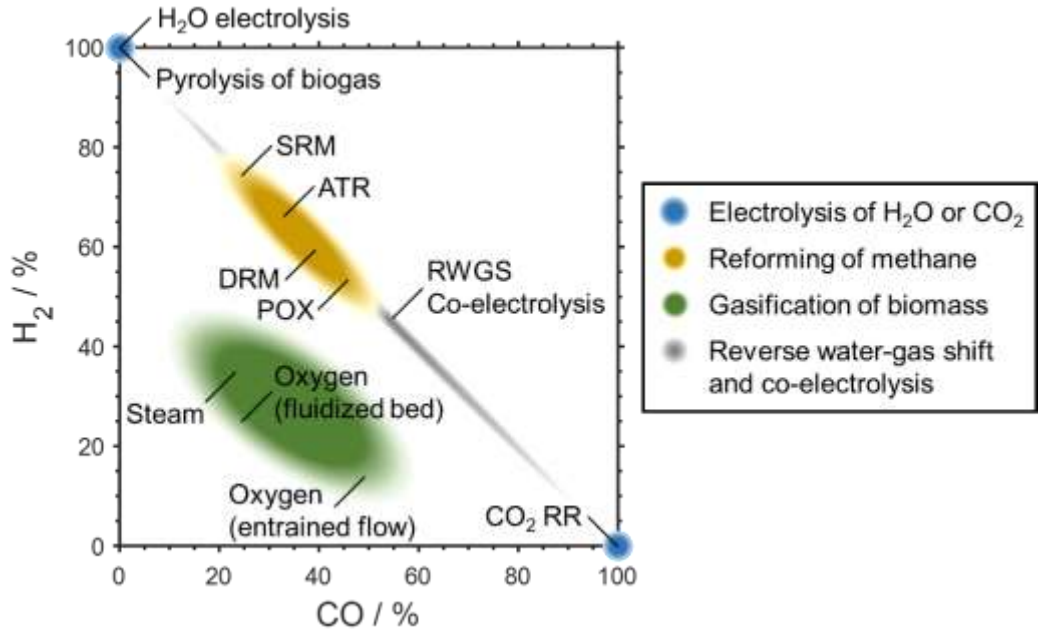

Figure 11.2 *Typical dry syngas compositions using carbon dioxide (CO_2; RR – reduction reaction; RWGS – reverse water-gas shift), water (H_2O), methane (SRM – steam reforming; ATR – autothermal reforming; DRM – dry reforming; POX – partial oxidation), and biomass as feedstock.*

With respect to the production of SAF, alternative routes must be used for the supply of sustainable syngas. Defossilisation of syngas production demands alternative carbon and hydrogen sources. The refinery of the future, which has been described by Vogt and Weckhuysen[27], may solely rely on CO_2, biomass, and plastic waste as carbon feedstock while using water (H_2O) as hydrogen feedstock. To produce SAF from CO_2 as carbon feedstock, biogenic sources or direct air/ocean capture (DAC/DOC) represent idealised solutions. However, unavoidable CO_2 from industrial flue gases, such as cement plants, biogas, or captured CO_2 from other point sources represent a good intermediate solution, but carbon capture utilisation (CCU) strongly depends on local availability, legislation, regulation, and economic incentives[28]. Abundant electricity from renewable sources must be provided to enable electrification of individual process steps and electrocatalytic activation of CO_2 and H_2O (see Figure 11.3). Syngas may be produced via electrolysis of water (Eq. 11.1) and catalytic reduction of CO_2 (Eq. 11.2) or in a combined co-electrolysis (Eq. 11.3). While water

splitting is already commercialised on large scale, the latter processes represent immature technologies with increased electricity demand[29] that nevertheless offer great potential to simplify the processes for future SAF production (see Figure 11.4). The RWGS reaction (Eq. 11.4) represents a solution for CO_2 activation available today even though hardly any large-scale commercial plants exist.

$$2H_2O_{(l)} \rightarrow 2H_{2(g)} + O_{2(g)} \quad (11.1)$$

$$2CO_{2(g)} \rightarrow 2CO_{(g)} + O_{2(g)} \quad (11.2)$$

$$CO_{2(g)} + H_2O_{(g)} \rightarrow H_{2(g)} + CO_{(g)} + O_{2(g)} \quad (11.3)$$

$$CO_{2(g)} + H_{2(g)} \rightarrow CO_{(g)} + H_2O_{(g)} \quad (11.4)$$

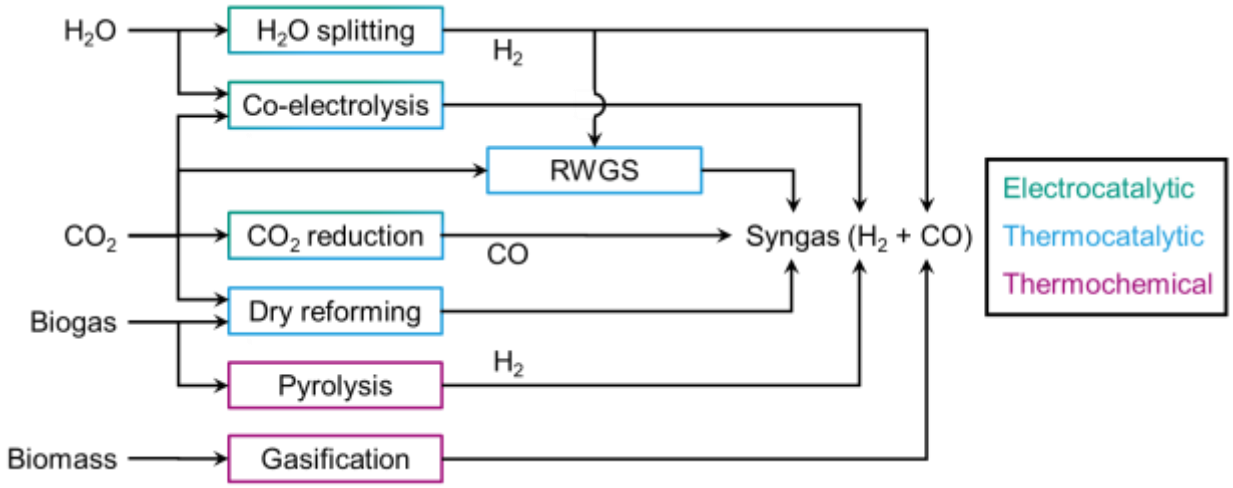

Figure 11.3 *Electrocatalytic, thermocatalytic, and thermochemical production pathways for sustainable syngas for the production of SAF via the Fischer-Tropsch synthesis based on biogenic feedstock, carbon dioxide (CO_2), and water (H_2O).*

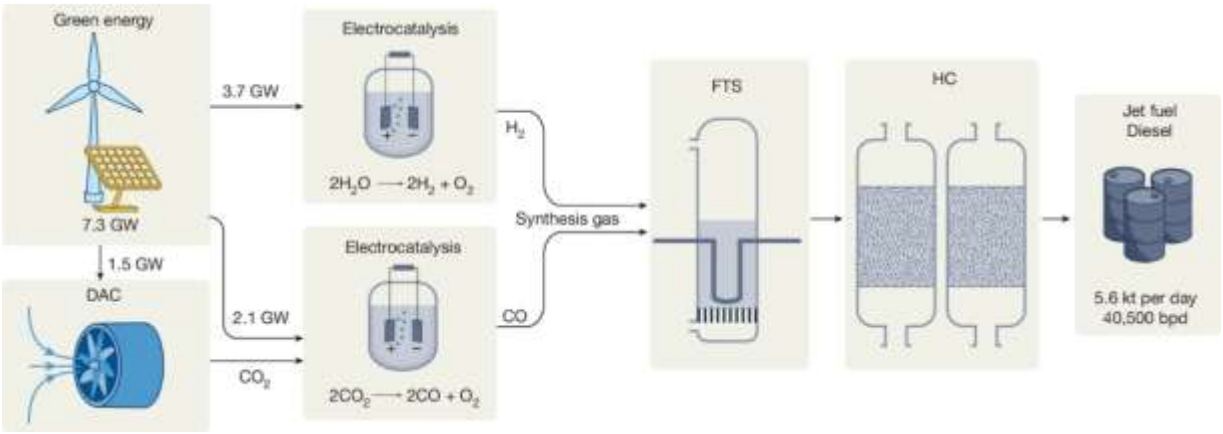

Figure 11.4 *Potential scenario for a future production of synthetic fuels via fully electrified production of syngas (H_2 and CO) using water (H_2O) and carbon dioxide (CO_2) from direct air capture (DAC) with subsequent Fischer-Tropsch synthesis (FTS) and product make-up via hydrocracking (HC).* **Reproduced from ref. 27 with permission from Springer, Copyright 2024.**

Biogenic feedstock, such as waste biomass, food waste, or biogas, represents a combined carbon and hydrogen source for the production of syngas (see Figure 11.3), while the H_2:CO ratio may be too low and require additional H_2 (see Figure 11.2). Further, biomass has a high oxygen content and the potential for using biogenic feedstock is restricted to certain regions, where it may play a crucial role in the energy system. Mature technologies already exist for the production of bio-based SAF and bio fuels, namely for hydroprocessed esters and fatty acids (HEFA) as well as hydrotreated vegetable oil (HVO), respectively. With respect to SAF production via the FT route, gasification of biomass and reforming of biogas may provide sustainable syngas in a first step (see Figure 11.2). However, the potential of PTL is several magnitudes higher due to the enormous renewable energy reserves[26], but commercial implementation is not as mature yet.

Another important aspect for the sustainable production of syngas is the mode of energy input into catalytic reactors, which is required during start-up and, more importantly, to drive the typically endothermic reactions. Here, electrified heating approaches using renewable energy may replace the conventional use of fossil fuels, such as combustion of natural gas. A broad

range of approaches is currently developed and focuses, amongst others, on RWGS and reforming of methane[30-33]. Noteworthy, first pilot and demonstration plants for large-scale implementation of electrified heating are operated in the chemical industry[30, 34, 35].

11. 2. 2. Gasification of biomass

The feedstock, H_2 and CO, for the FT process can be produced from coal, natural gas, petroleum coke, biomass, wood pellets, agricultural residues, plastic, or waste material via gasification[5, 36]. The feedstock and method of gasification influences the composition of the produced syngas. During gasification, the feedstock is partially oxidized at high temperatures ranging from 800 to 1000 °C with oxygen (O_2) or steam (H_2O)[37]. The overall reaction for the gasification of a simplified feedstock C_nH_m with O_2 (Eq. 11.5) yields an equimolar syngas with an H:C ratio of 2:1, *i.e.,* 2n = m. Lignin and cellulose rich biomass, which is the common feedstock for the gasification of biomass, have a H:C ratio of approx. 1.5:1, which consequentially results in H_2:CO ratio below 1:1 in the produced syngas. This strong dependence of the syngas composition on the chemical composition of the feedstock can be overcome with the direct addition of water to the gasification process or a subsequent WGS stage (Eq. 11.6), which comes at the expense of loss of carbon source via production of CO_2. Hence, combination with sustainable H_2 sources is the preferred process.

$$2C_nH_{m(s)} + nO_{2(g)} \rightarrow 2nCO_{(g)} + mH_{2(g)} \quad (11.5)$$

$$CO_{(g)} + H_2O_{(g)} \rightarrow CO_{2(g)} + H_{2(g)} \quad (11.6)$$

Gasification of solid carbonaceous materials involves pyrolysis forming volatile gases, liquids, oxygenates, and char, which is subsequently converted via gas phase and char-gas reactions (see Figure 11.5). The chemical reactions involve (partial) oxidation with O_2 (Eq. 11.7 – 11.9), the Boudouard reaction (Eq. 11.10), water-gas reaction (Eq. 11.11), and methanation of carbon (Eq. 11.12). Further, the homogeneous gas phase reactions via WGS (Eq. 11.6) and steam reforming of methane (Eq. 11.13) take place[38].

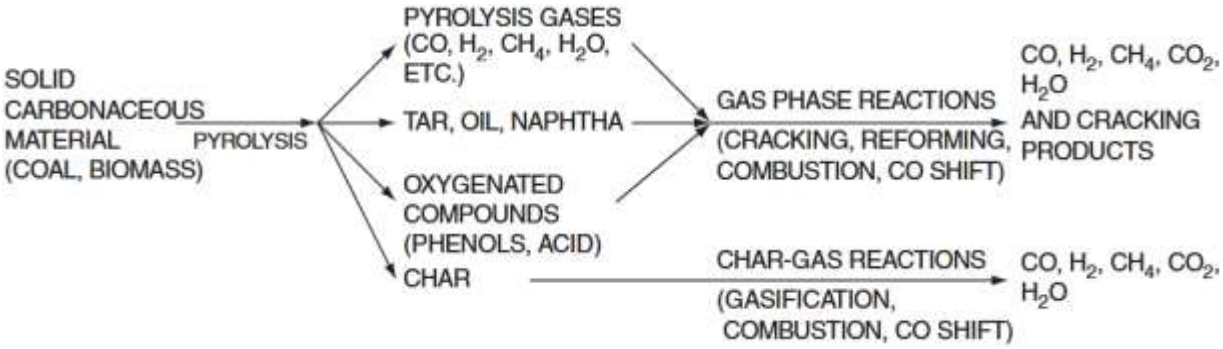

Figure 11.5 *Gasification of biomass.* **Reproduced from ref. 39 with permission from Elsevier, Copyright 2008.**

$$2C_{(s)} + O_{2(g)} \rightarrow 2CO_{(g)} \quad (11.7)$$

$$2CO_{(g)} + O_{2(g)} \rightarrow 2CO_{2(g)} \quad (11.8)$$

$$2H_{2(g)} + O_{2(g)} \leftrightarrow 2H_2O_{(g)} \quad (11.9)$$

$$C_{(s)} + CO_{2(g)} \rightarrow 2CO_{(g)} \quad (11.10)$$

$$C_{(s)} + H_2O_{(g)} \rightarrow CO_{(g)} + H_{2(g)} \quad (11.11)$$

$$C_{(s)} + 2H_{2(g)} \rightarrow CH_{4(g)} \quad (11.12)$$

$$CH_{4(g)} + H_2O_{(g)} \rightarrow CO_{(g)} + 3H_{2(g)} \quad (11.13)$$

The biggest challenge for biomass gasification is the low energy density and the high ash content of biomass, which requires larger gasifiers for BTL. In particular, the low energy content of biomass contradicts the required large-scale FTS plants in order to reach commercial viability, which represents a major challenge for economic viability. The energy density can be increased by co-feeding of non-biogenic materials, such as polymers[40]. Alternatively, biosyncrude can be produced in a separate pyrolysis step to increase the energy density[41]. The latter strategy has been implemented in the bioliq© concept at Karlsruhe Institute of Technology (KIT), which has been constructed between 2005 and 2013[42]. Decentralised fast pyrolysis of low energy biomass, such as straw, was combined with centralised high

pressure entrained flow gasification (see Figure 11.6), while the pilot plant also comprised syngas clean-up and the production of fuels. The biosyncrude consists of the pyrolysis oil with up to 40 wt.% of pyrolysis coke yielding a tenfold increase in energy density, which enables efficient transportation to the centralised gasification[42, 43]. Since 2025, part of the bioliq© process has been transferred to the Carbon Cycle Lab (CCLab), which extends the feedstock for pyrolysis to polymers[44].

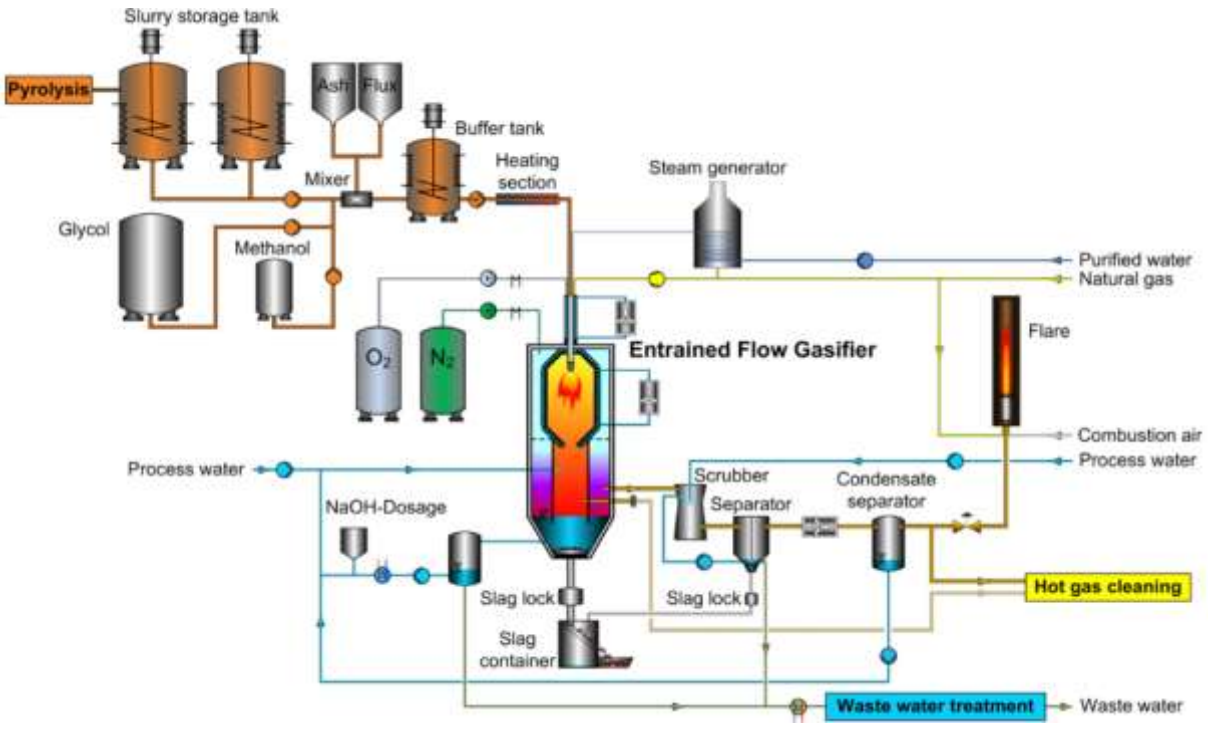

Figure 11.6 *Process flowsheet of the bioliq© process at Karlsruhe Institute of Technology (KIT) using a combination of fast pyrolysis of biomass and high-pressure entrained-flow gasification.* **Reproduced from ref. 43, https://doi.org/10.1002/cben.202000006, under the terms of the CC BY 4.0 license https://creativecommons.org/licenses/by/4.0/.**

After the gasification process, various steps of gas cleaning, purification, and adjustment of the H_2:CO ratio of the produced syngas is required before being used in the FT process (see Figure 11.7). In fact, cleaning of syngas is considered the biggest challenge and also a major driver for costs of SAF production via the BTL process[45]. Aside from tar, particulate matter, and trace amounts of metals, syngas from biomass gasification typically contains common

catalyst poisons, such as NH_3, HCN, H_2S, COS, CS_2, or HCl[45-47]. FT catalysts are extremely sensitive to such impurities, which often cause irreversible deactivation[45]. Further, CO_2 and CH_4 represent the major side products while N_2 may be prominent for gasification with air, which affects the concentration of H_2 and CO in the syngas (see Figure 11.2) and, in the case for CO_2, may also be detrimental to the catalyst selectivity[45, 47].

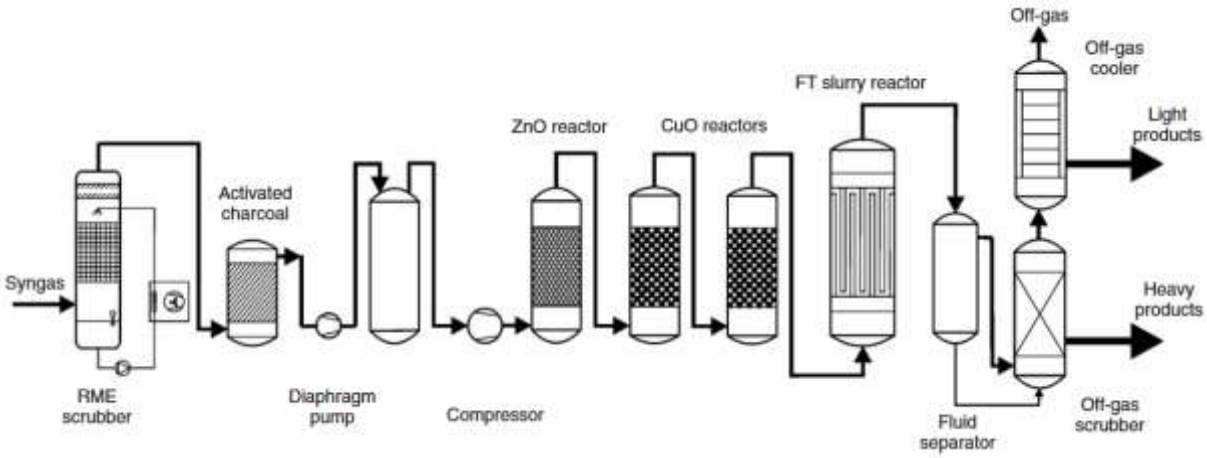

Figure 11.7 *Process flowsheet of the Fischer-Tropsch synthesis in Güssing based on syngas production via steam gasification of biomass in a dual fluidised bed reactor.* **Reproduced from ref. 48 with permission from John Wiley and Sons, Copyright 2013.**

The cost and efficiency of the gasification process depends on the type of feedstock, reactor designs, and more. Examples of further research into realising and up-scaling such processes can be found in comparative studies, indicating the cost of waste tire gasification to syngas and FT process to SAF estimated around $0.66 USD/L with potential environmental impacts[36]. The ability of applying versatile feedstock into the gasification process is one of the advantages of optimizing this process into the carbon-neutral syngas pathway of producing SAF. Many examples exist for demonstration plants for the BTL process. However, only a few large-scale plants are in operation. Already in 1998, Choren Industries commissioned the Carbo-V® pilot plant in Freiberg, Germany, which was later extended with an FT stage in 2000. In Güssing, Austria, a steam gasifier for wood chips serves as a platform for the development of downstream technologies including FTS since 2002 (see Figure 11.7).

11. 2. 3. Reforming of Biogas

Biogas can be produced from a diverse range of feedstocks, including organic materials and waste from agriculture, forestry, and municipality. Biogas generally contains CH_4, CO_2, N_2, O_2, H_2O, and trace amounts of other gases depending on the feedstock with CH_4 and CO_2 being the main components.

Steam reforming of methane (SRM, Eq. 11.13) and pyrolysis (Eq. 11.14) are applicable for conversion of the CH_4 fraction to syngas and H_2, respectively (see Figure 11.2). SRM can leverage existing small-scale technologies for reforming, which has been implemented in a range of demonstration plants[49]. In addition, first electrified reactors for SRM are under development[33, 35]. Several approaches on the pyrolysis of CH_4 for the production of biogenic H_2 and industrial grade carbon have been developed. Separation of the solid carbon and operational stability represent common challenges, which may be overcome by using highly dynamic reaction engineering solutions, such as liquid metal reactors. However, the typically composition of biogas lies in the range of 50% to 70% CH_4 with the balance being mostly CO_2, which makes it an ideal feedstock for dry reforming of methane (DRM, Eq. 11.15)[50].

$$CH_{4(g)} \rightarrow C_{(s)} + 2H_{2(g)} \quad (11.14)$$

$$CH_{4(g)} + CO_{2(g)} \rightarrow 2CO_{(g)} + 2H_{2(g)} \quad (11.15)$$

During DRM, CO_2 replaces steam as oxidant when compared to SRM. Actually, DRM is expected to have approx. 20% lower operating costs in comparison to SRM[51]. DRM generates syngas with a H_2:CO ratio of ~1:1 (see Figure 11.2). Environmentally friendly sources are landfill gas and biogas, which are gas mixtures originated from microbial action. DRM is highly endothermic in comparison to SRM, which makes elevated temperatures in the range of 700 to 1000 °C inevitable in order to reach a satisfactory syngas yield[52]. The RWGS reaction (Eq. 11.4) is the major side reaction of DRM and the main cause for a H_2:CO ratio below equimolarity[53].

DRM has not been applied in large-scale production yet, as it still lacks economic attractiveness. Major challenges are rapid catalyst deactivation due to carbon deposition, sintering of the catalyst, high energy demand for elevated temperatures, need for pure feedstock, and side reactions[54]. However, a few industrial processes have been developed and particularly attempted to tackle the coking challenge either on a process scale via co-feeding H_2O or via the development of coke resistant catalysts. Nevertheless, they are still not optimal, presenting limitations in regards to the applicability to many downstream processes[51].

The sulphur passivated reforming (SPRAG) was developed by Topsoe (Sterling Chemicals Inc.; USA) in 1987[55, 56]. It combines DRM and SRM by adding steam to the feed stream, allowing a variety of H_2:CO ratios to be obtained[57]. The Industrial Caloric Process (CALCOR) was developed by Caloric GmbH in Germany in 2000 and is based on CO_2 as the sole oxidant. A large excess of CO_2 results in H_2:CO ratios even below 1:2. In addition to the excess of CO_2, the process circumvents coking by operating close to atmospheric pressure[51, 58]. DRYREF is a technology established by Linde and BASF, Germany, together with partners in 2018. Linde scaled-up dry reforming to a pilot reformer in 2017, which could be used at commercial levels with a syngas capacity of 50 000 $m_N^3\ h^{-1}$. DRYREF aims at improving the carbon footprint of syngas production by lowering the steam content on the feed stream and adding CO_2. Hence, this is a dual process as it is based on SRM but with an option to incorporate CO_2 feedstock, which may provide H_2:CO ratios exceeding 1:1. Aside from the presence of steam, deactivation of the catalyst by coking was overcome by the tedious development of a new catalyst, the Ni-based SYNSPIRE™ G1-110, by BASF[59].

11. 2. 4. Reverse Water-gas Shift Reaction

The RWGS reaction (Eq. 11.4) provides great potential for the production of clean syngas based on CO_2 and H_2 (see Figure 11.3), but only a few processes via thermocatalytic routes have been implemented on a commercial scale[60]. The name is indicative for the reversed reaction direction of the established WGS reaction (Eq. 11.6) used for the adjustment of the syngas composition or the complete shift towards pure H_2 in the case of the Haber-Bosch

process. As the gas mixture during RWGS is composed of CO_2 and CO rich syngas, hydrogenation of CO_x represents the main side reaction, in particular the methanation of CO_2 (Eq. 11.16)[61]. Once CO is formed, the methanation of CO (Eq. 11.17) represents another major side reaction lowering the carbon yield in the syngas. The endothermic RWGS requires high operation temperatures to enable reasonably high conversion levels (see Figure 11.8). While the exothermic methanation reactions may be effectively suppressed at operation temperatures exceeding 800 °C, the equilibrium conversion of the pressure insensitive RWGS reaction can only be increased with higher H_2:CO_2 ratios and temperatures[62, 63]. A higher H_2 concentration in the feed can easily be implemented as a H_2:CO ratio of 2:1 is often targeted for the produced syngas, which is also the case for the FTS. Hence, unconverted H_2 from the RWGS stage may be used to adjust the syngas composition. However, increasing the H_2:CO_2 ratio also favours methanation. Higher temperatures facilitate decomposition of potentially formed methane (Eq. 11.14), but may lead to a further side reaction via the (reversed) Boudouard reaction (Eq. 11.10 and 11.18). Lastly, syngas for the FTS is required at elevated pressures of approx. 20 bar, which demands for the syngas production at increased pressure levels or, less attractive, an energy intense compression stage before the downstream processes[61, 63].

$$4H_{2(g)} + CO_{2_{(g)}} \rightarrow CH_{4(g)} + 2H_2O_{(g)} \quad (11.16)$$

$$3H_{2(g)} + CO_{(g)} \rightarrow CH_{4(g)} + H_2O_{(g)} \quad (11.17)$$

$$2CO_{(g)} \rightarrow C_{(s)} + 2CO_{2(g)} \quad (11.18)$$

This discussion of the thermodynamics of the RWGS reaction already demonstrates some of the challenges for large scale implementation. The catalysts for RWGS must either kinetically hinder methanation at low reaction temperatures, *i.e.*, provide a high CO selectivity while suppressing hydrogenation of CO_2 and CO, or show a high thermal resistance for operation at high temperatures[61, 63]. For example, widely applied copper-based catalysts effectively suppress methanation due to a hindered dissociation of CO on the catalyst surface. Aside

from copper (Cu), noble metal catalysts, such as platinum (Pt) and rhodium (Rh), are often applied for low-temperature (250-500 °C) RWGS, while metal oxide-based catalysts, such as zinc oxide (ZnO), indium (III) oxide (In_2O_3), or perovskites, represent alternatives for higher operation temperatures (700-900 °C) and the intermediate regime (500-700 °C)[61, 62].

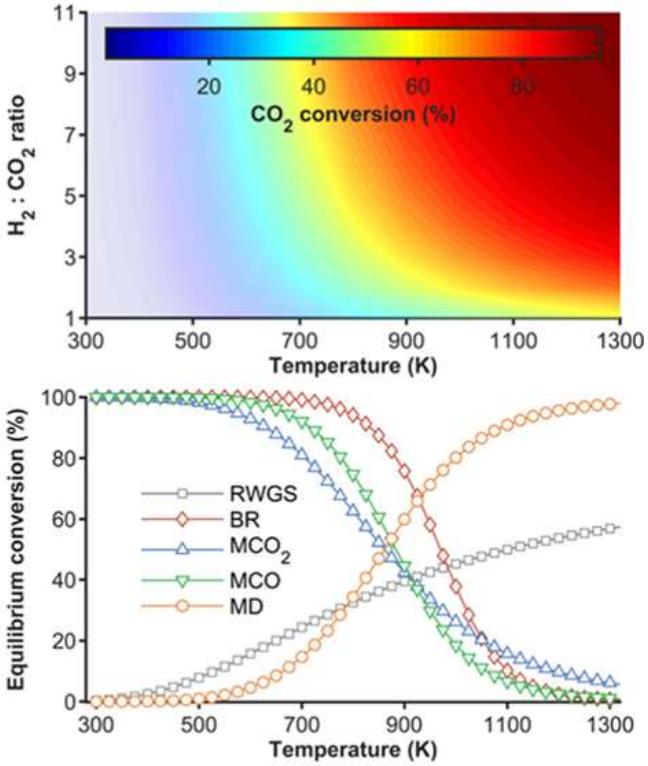

Figure 11.8 *Individual equilibrium conversions of the reverse water–gas shift and side reactions (BR – Boudouard reaction; MCO_2 – methanation of CO_2; MCO – methanation of CO; MD – methane decomposition) as a function of temperature at 1 bar (top). Effect of H_2:CO feed ratio and temperature on the equilibrium conversion of reverse water–gas shift at 1 bar (bottom).* **Reproduced from ref. 63 with permission from the American Chemical Society ACS, Copyright 2021.**

Advanced reactor solutions including product separation may optimise energy efficiency and tackle the limitations with respect to thermodynamics for efficient CO_2 conversion via the RWGS reaction. Here, the development of membrane reactors for *in situ* removal of H_2O are at the core of these emerging technologies. Further, chemical looping provides great potential and represents an elegant solution for process intensification for the RWGS reaction[60].

Emerging reactor technologies also include electrified heating towards a holistic sustainable process design for the production of sustainable syngas[30, 31].

11.3 Fischer-Tropsch Synthesis

11. 3. 1. Process

FTS is a series of chemical reaction that transforms syngas, a mixture of CO and H_2, into hydrocarbons and water (Eq. 11.19). FTS produces a broad spectrum of hydrocarbons, up to 100 carbons, such as, paraffins, olefins, oxygenates, and aromatics. The classic FT process includes four steps: syngas generation, syngas cleaning, FTS, and product upgrading (see Figure 11.9).

$$CO + 2H_2 \rightarrow (CH_2) + H_2O \quad (11.19)$$

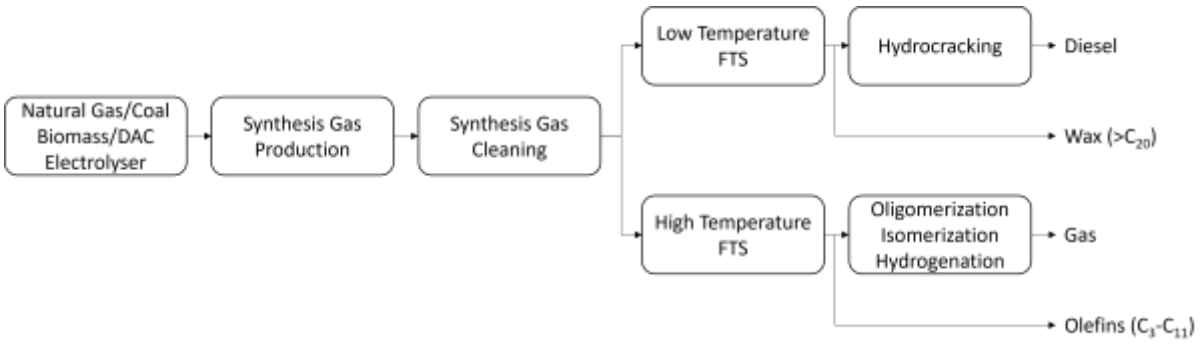

Figure 11.9 *Overall scheme for the production of synthetic liquid fuels and other hydrocarbon products via FT process.* **Reproduced from ref. 17 with permission from the John Wiley and Sons, Copyright 2008.**

Conditioning of the downstream flows containing both, unconverted educts and products, is inevitable to improve yields of desired products. Gaseous hydrocarbons are mostly reformed to synthesis gas and recycled together with unconverted or dissolved synthesis gas via mixing points with fresh synthesis gas upstream of the reactor. This recycle flow is relatively high when compared to other syntheses[10], because the per-pass syngas conversion during FTS is

often limited due to heat removal constraints. Alternatively, the C_1-C_4 products already represent a saleable product. The final product conditioning of liquids includes distillation columns for the separation into several boiling point fractions and cracking of long-chain waxes to the desired carbon chain lengths for diesel. Most of the required post-treatment processes are known from conventional petroleum refineries[64].

11. 3. 2. Reactors

The development of reactor configurations has evolved in parallel with the demands of industrial scalability, catalyst stability, heat management, and the compatibility with sustainable syngas sources derived from biomass, other biogenic feedstock, water, and/or CO_2 reduction. This section presents a detailed overview of reactor design history, performance comparisons, and emerging technologies, with a particular focus on the transition from large-scale systems to modular, micro-structured reactors suitable for decentralised applications.

The earliest industrial implementation of low temperature Fischer-Tropsch synthesis (LTFTS), by Sasol in South Africa, was based on multi-tubular fixed-bed reactors. These reactors consist of thousands of narrow tubes filled with iron-based catalyst pellets, surrounded by a circulating heat-transfer medium, such as Dowtherm oil or pressurised water, to remove the substantial reaction heat. This configuration enabled excellent thermal control and facilitated large-scale production from coal-derived syngas[11, 65]. The fixed-bed reactors at Sasol were at that time among the largest ones in the world, with individual reactors exceeding 600 m^3 in volume, which back then contributed significantly to the global synthetic fuel output. However, fixed-bed reactors have limitations, such as the temperature gradients inside the catalyst tubes, which can cause sintering and deactivation. Furthermore, single train fixed-bed reactors are inflexible under variable load conditions and rapid start-up/shut-down cycles, which makes them less suitable for syngas derived from intermittent renewable sources[66]. To overcome these limitations, slurry-phase bubble column reactors (SBCRs) gained industrial attention in the 1990s and 2000s. In SBCRs, fine catalyst particles are suspended in a wax-like liquid

medium while syngas is bubbled through, offering excellent heat removal from the liquid phase to cooling coils and uniform temperature profiles[67]. However, challenges such as catalyst filtration, slurry handling, and product separation complicate scale-up and long-term operation[68]. Fluidised-bed reactors, including fixed fluidised-beds (FFBRs) and circulating fluidised-beds (CFBRs), improve mass transfer while allowing for continuous catalyst regeneration. However, fluidised-bed systems are mechanically complex, requiring solids handling and erosion-resistant materials under pressurised operation.

The current shift toward decentralised production, particularly for synthetic fuels, *e.g.,* for use as SAF, derived from captured CO_2 and green hydrogen, has prompted the development of micro-structured and modular FT reactors. These systems are inherently better suited for dynamic operation with variable renewable energy sources. A modular nature of reactor systems also supports load flexibility. Studies indicate that operation under fluctuating loads, similar to the diurnal pattern of photovoltaic energy, can be achieved through step changes in feed rates of 20% without compromising product distribution or catalyst performance[69]. Moreover, such systems are amenable to one-pass operation, minimizing the complexity of recycle loops and separation units. Automated control enables rapid adaptation to input variability while maintaining optimal reaction conditions.

The compact advanced non-slurry reactor from JM and bp (FT CANS™) is a notable example of modular FT reactor technology combining advantages from slurry with fixed-bed reactors to maximise productivity[70]. Velocys Inc. has developed microchannel FT reactors with high surface-to-volume ratio to ensure efficient heat management, substantially greater than conventional reactors. This design allows the system to operate at high conversion per pass and sustain long catalyst lifetimes without temperature runaway[71]. Microchannel reactors have demonstrated twice the thermal efficiency of traditional fixed-bed systems due to optimised heat utilisation and preventative heat losses[72]. German company INERATEC has advanced this concept further by commercialising compact plug-flow tubular reactors for FTS, integrating them into PTL pilot plants. These reactors typically operate at 20–25 bar and 210–220 °C,

with high-performance and compact heat exchange microstructures. The design supports rapid start-up/shut-down, small footprint installation, and compatibility with modular hydrogen and CO_2 capture units[73]. INERATEC reactors represent a scalable solution for synthetic fuel production at decentralised sites such as airports, remote industrial parks, or biogas facilities.

The conversion in the FTS and the gas phase composition can be described by the partial pressure ratio of the product water to the reactant hydrogen (p_{H2O}/p_{H2})[74], which follows an exponential dependency on the FT conversion level (see Figure 11.10). Water, an oxidising agent, opposes the reducing atmosphere of synthesis gas, which becomes challenging at high conversion levels. Historically, the high concentration of water was, alongside the strong exothermic nature of the FTS, a major challenge for FT processes. The development of SBCRs and micro-structured reactors with superior heat control alongside sophisticated and adapted catalyst development for superior hydrothermal stability pushed, amongst other factors, the operational limits to 90%. In particular further advancement in catalyst optimisation, *e.g.,* for use in modular plants such as micro-structured reactors, may enable even higher conversion levels. However, the gain in conversion is small compared to the associated drastic increase in the partial pressure of water (see Figure 11.10). Separation of H_2O from the reaction mixture during recycle or in the reactor by using membranes or sorption enhanced processes represents an alternative approach for operation at high per-pas conversions[75, 76], but has not been demonstrated on large scale.

A comparison across LTFTS reactor configurations highlights distinct trade-offs. Multi-tubular fixed-bed reactors offer unparalleled scalability and mature engineering, but are less flexible and prone to thermal maldistribution. Slurry-phase reactors ensure uniform temperature control, but face mechanical and operational constraints related to catalyst separation. Fluidised systems promise high throughput and regeneration capacity, yet require advanced mechanical integration. In contrast, micro-structured reactors combine thermal efficiency, load flexibility, and compactness, which are essential features for next-generation FT applications.

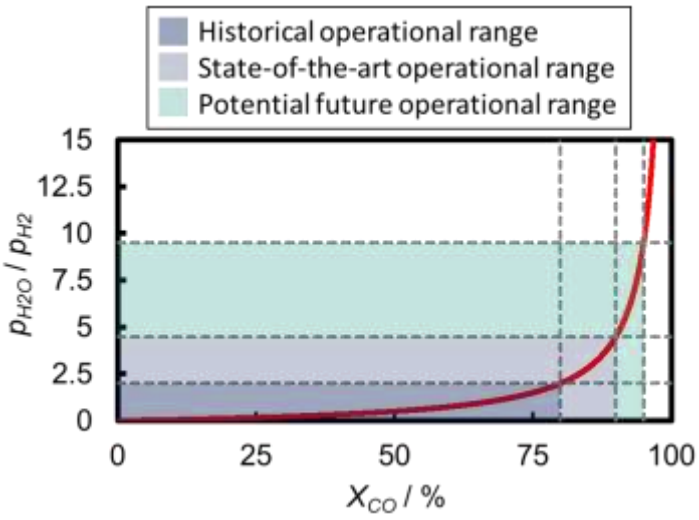

Figure 11.10 *Theoretical dependence of partial pressure ratio of water (H_2O) to hydrogen (H_2) on the conversion level of carbon monoxide with historical (up to 80% conversion), state-of-the-art (up to 90% conversion) and potential future (up to 95% conversion) operational ranges for the Co-based low temperature Fischer-Tropsch synthesis. A feed gas composition and stoichiometric consumption of H_2:CO of 2:1 without the formation of any gaseous hydrocarbons are underlying assumptions.*

From a performance point of view, the targeted chain-growth probability (α) in LTFTS is high across all reactor types, often in the range of 0.9 or higher for cobalt catalysts, which results in the production of waxy hydrocarbons. Refining of FT crudes allows for an enhanced control over the overall product yields, which is more efficient than modulation of FTS for large production sites[77]. With respect to FT reactors, the selectivity can be tuned more precisely in micro-structured systems due to a superior temperature control and uniform residence time distributions. Activity per unit volume tends to be highest in microchannel and fluidised-bed reactors, given the enhanced mass transfer and higher space velocities[11, 78].

In conclusion, the choice of reactor design for cobalt-based LTFTS depends not only on production scale and desired product, but also increasingly on integration potential with renewable energy systems. The continued evolution of reactor technology, especially the emergence of compact, flexible, and high-efficiency systems, will be essential to meet the

defossilisation goals of future fuel production via FTS. These reactor innovations provide a critical foundation for deeper exploration into the fundamental catalytic processes that influences FT performance. However, established large-scale reactor concepts remain important for the production of the immense quantities of SAF required (see Figure 11.1) to transform aviation sector, in particular for processes based on steady production of large volumes of syngas.

11. 3. 3 Reaction Mechanism and Product Distribution

The reaction mechanism of FTS consists of three stages to produce a broad range of hydrocarbon products, which includes formation of the hydrocarbon chain initiator, chain propagation (growth), and chain termination (product desorption). The stoichiometry of the overall, generalised FT reaction for hydrogenation of CO forming hydrocarbon chain segments (CH_2) and H_2O demands a 2:1 ratio of H_2:CO (Eq. 11.19)[79, 80]. The more specific reaction equations for the formation of paraffins and olefins can be generalised as well (Eq. 11.20 and 11.21)[81].

$$nCO + (2n + 1)H_2 \rightarrow C_nH_{2n+2} + nH_2O \quad (11.20)$$

$$nCO + 2nH_2 \rightarrow C_nH_{2n} + nH_2O \quad (11.21)$$

The average chain length of the hydrocarbon product is influenced by the stoichiometric composition of CO and H_2 in the feed gas[11, 82]. Additionally, the side reactions of FT process, methanation (Eq. 11.17) and WGS reaction (Eq. 11.6), also influence the produced range and distribution of hydrocarbons.

CH_4 is a thermodynamically stable hydrocarbon product under FT reaction conditions. Temperature, pressure, feed gas composition, and the catalyst are all factors that influence the chain propagation step in the FT reaction mechanism resulting in different hydrocarbon product distributions (see Figure 11.11). Derived from the statical model of polymerisation, the Anderson-Schulz-Flory (ASF) model is used to describe the hydrocarbon product distribution during FTS using α (Eq. 11.22)[78, 83].

In the ASF model, the molar fraction of the hydrocarbon product with N carbons (M_N) can be determined by the molar fraction of C_1 products (M_1) multiple by α to the power of $N-1$. By plotting $\log M_N$ against N, the hydrocarbon yields from the FT reaction can be described by α, which represents the slope. In order to industrially produce long-chain hydrocarbons for products such as SAF in LTFTS conditions, α values exceeding 0.9 are targeted for economic viability even though an α value of 0.84 provides the maximum share of kerosene[77]. Maximising SAF yields is easier during the product make-up, which is, aside from minimising the formation of short-chain hydrocarbons below the SAF range, the reason for the desired higher chain growth probabilities during FTS. This can be exemplified when comparing the maximum yield of kerosene of 40% according to the ASF distribution, while production sites for SAF via FTS including product make-up may achieve an overall yield of 80%[84, 85]. In high temperature Fischer-Tropsch synthesis (HTFTS), α typically ranges between 0.65 and 0.75[77, 78].

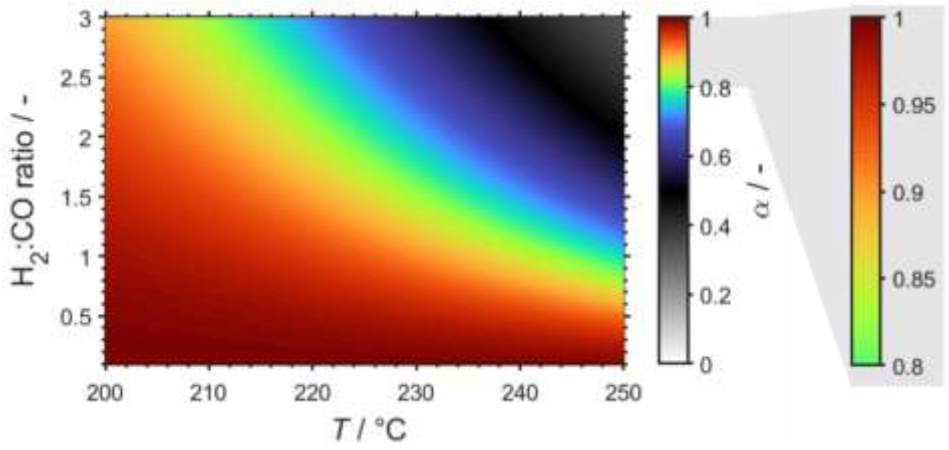

Figure 11.11 *Dependence of the hydrocarbon chain-growth probability (α) on temperature (T) and syngas composition for a cobalt-based Fischer–Tropsch catalyst using a single α selectivity model and parameters from ref. 86 for the pressure range 12 to 36 bar.*

$$M_N = M_1 * \alpha^{N-1} \quad (11.22)$$

11. 3. 4. Catalysts

Catalysis lies at the core of chemical process intensification. Heterogeneous catalysis allows for the transformation of gaseous carbon oxides and H_2 into valuable hydrocarbon products through surface-mediated mechanisms[83]. These transformation occur through a sequence of molecular adsorption onto the solid catalyst surface, migration to the active sites/phases, bond activation, rearrangement, desorption of products and the regeneration of the catalytic surface[79]. The critical sites for these reactions are often on the edges, terraces, vacancies or ensembles of metal surfaces, where bond breakage and formation are energetically favoured[87].

The FTS requires a metal-based catalyst to enable CO hydrogenation[2, 88]. Fe and Co are currently the industrially viable FT catalysts. Fe-based FT catalyst provide a better performance at the higher reaction temperature range during HTFTS but also LTFTS, while Co-based FT catalysts are exclusively used at lower temperatures in the range of 220 to 270 °C[81]. Fe-based catalysts have a high WGS activity (Eq. 11.6), which allows for using hydrogen poor syngas from coal gasification. The cost efficiency of different catalysts is compared by the catalytic activity per unit of catalyst mass and its lifetime. While Fe-based FT catalyst benefits from the low cost of material, Co-based FT catalyst typically enable higher productivity at increased conversion rates[89]. In the 1930s, a Co-based FT catalyst promoted by thorium (Th), zirconium (Zr), magnesium (Mg), and/or mixed with Kieselguhr, a siliceous sedimentary rock, was first developed and commercialised in a German-based CTL plant[90]. Currently, Co-based FT catalysts are usually supported by metal oxides with large surface area, such as alumina (Al_2O_3), silica (SiO_2), and/or titania (TiO_2)[91]. Pt, rhenium (Re), and ruthenium (Ru) are used as reduction promoters while lanthana (La_2O_3), zirconia (ZrO_2), and/or alkali oxides represent often used structural promotors. Catalytic systems are optimized through the choice and modification of support, promoter, and active phase. The support can disperse and stabilise the active metal while the promoter can provide structural or electronic functions to the reaction pathways. The active phase of a catalyst can influence

the activity and selectivity towards different hydrocarbon products, depending on the oxidation state, crystalline structure, and nanoparticle sizes[92]. In a Co-based FT catalyst, metallic cobalt (Co^0) is the catalytically active phase, generated from the two-step reduction from cobalt (II,III) oxide (Co_3O_4) to cobalt (II) oxide (CoO) and finally Co^0. Without thorough and careful reduction to generate the active phase, the reaction performance can be poor due to inactive oxides or particle sintering[93]. To fully utilise cobalt and overcome the higher material cost, the application of finely dispersed nanoparticles over supports with large surface area boosts the catalytic activity.

Application of a supported nano-sized cobalt phase goes along with various structural, surface-related features due to the unique physicochemical properties of nanoparticles[94]. Most importantly, a significant sensitivity of the FT activity and selectivity on the size has been identified for nanoparticles below 10 nm (see Figure 11.12). Such small nanoparticles exhibit a higher specific surface area, but may not expose all the required active sites for the FTS[95-97]. For example, the B_5B site has been proposed to be the most active site for CO dissociation. Its population in face-centred cubic (fcc)-Co nanoparticles increases with particle size and levels off above 8 nm[97]. Consequentially, a lower CO dissociation has been observed for smaller nanoparticles, which in turn results in a lower carbon coverage[95, 96]. In addition, step sites seemingly require relatively large terraces in order to tap their potential FT activity. Hence, small nanoparticles simply do not contain the required combination of step sites, terraces, etc. in order to compete with nanoparticles above 10 nm[97, 98], which demands for cobalt nanoparticle sizes larger than 8 to 10 nm for maximum productivity. Recent studies have also shown that the crystalline phases of cobalt, hexagonal closed-packed (hcp) and fcc, can influence the catalytic activity and stability during FTS[74, 99].

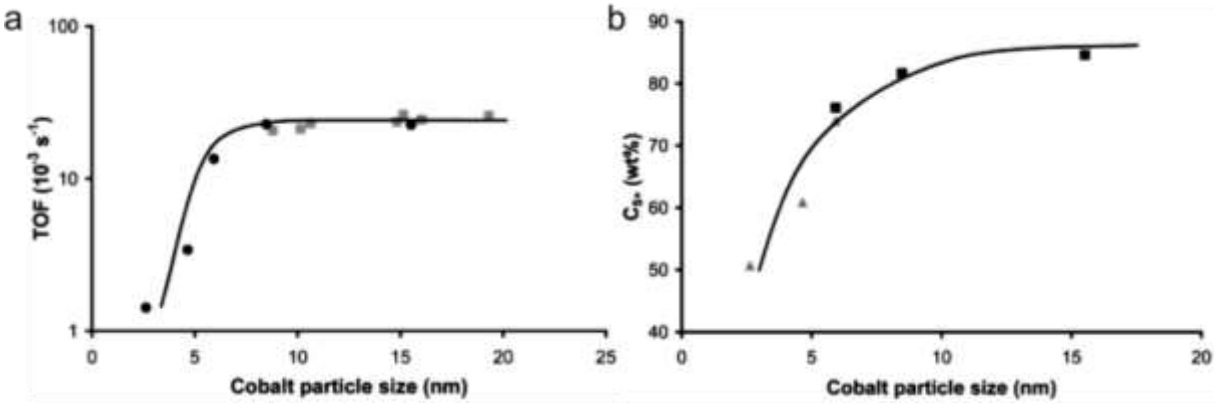

Figure 11.12 *Effect of cobalt nanoparticle size on (a) turnover frequency (TOF, black circles: Bezemer et al[98].; grey squares: Iglesia[100]) and (b) C_{5+} selectivity (black squares: 210 °C; grey triangles: 250 °C) under commercially relevant conditions.* **Reproduced from ref. 98 with permission from the American Chemical Society ACS, Copyright 2006.**

Gaseous water is a main product of the FTS as one molecule is formed for every carbon atom in the products. In turn, the concentration of water increases with the conversion (see Figure 11.10). In the gas phase, this effect is even more pronounced as most of the hydrocarbon products in the Co-based LTFTS are in the liquid phase under reaction conditions. The aforementioned need for increased hydrothermal stability of Co-based catalysts for operation at high per-pass conversion levels is mostly linked to suppression of re-oxidation of Co by water and sintering[101]. Both deactivation mechanisms can follow multiple pathways during FTS (see Figure 11.13). Re-oxidation to CoO may be suppressed for larger Co nanoparticles[101, 102], while sizes below 6 nm are prone to oxidation due to a lower surface energy of CoO nanoparticles[74]. As nanoparticles of ~10 nm size enable the most efficient use of cobalt due to the structural dependence of the FTS (see Figure 11.12), small nanoparticles should be avoided anyway.

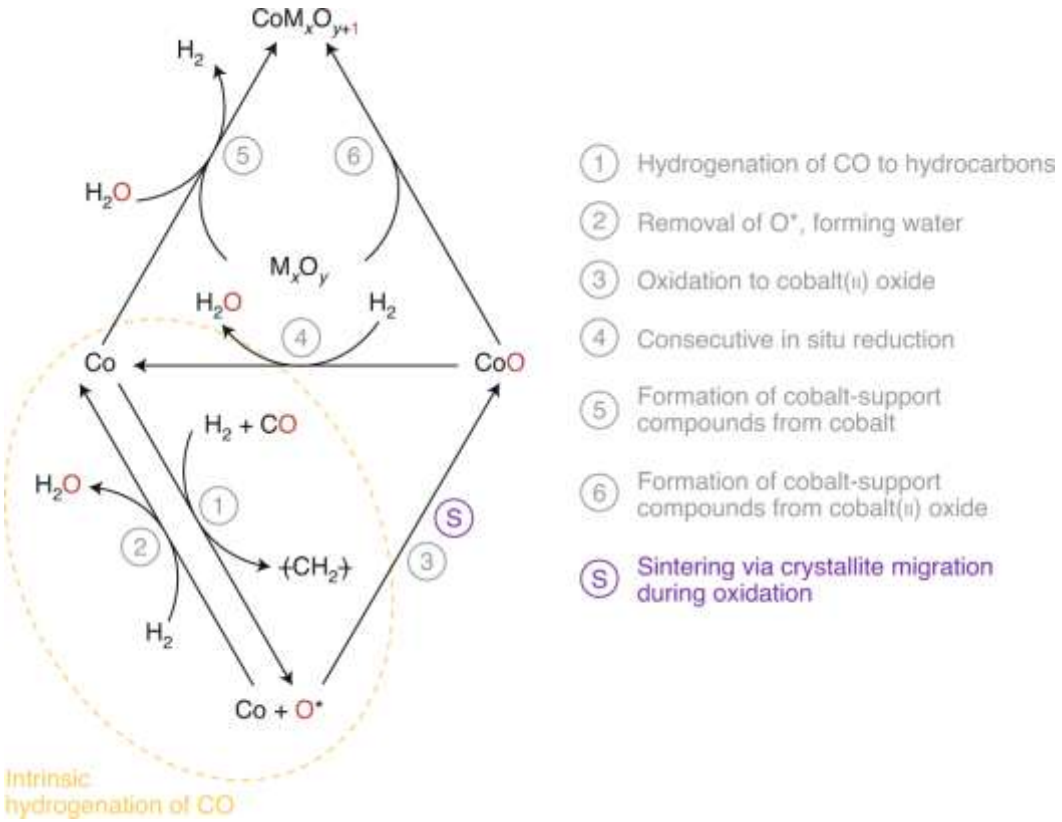

Figure 11.13 *Potential pathways of water-induced deactivation of cobalt-based catalysts in the Fischer–Tropsch synthesis (hydrogenation of CO according to reactions 1 and 2), with oxidation of cobalt to CoO (reaction 3), which may be associated with sintering (S). Consecutive in situ reduction of CoO to cobalt (reaction 4) or the formation of cobalt-support compounds with metal oxide carriers (MxOy; reactions 5 and 6).* **Reproduced from ref. 101.**

Re-oxidation via formation of metal-support compounds (MSCs) represents another pathway for water induced deactivation (see Figure 11.13)[91], but MSCs can already form during thermal treatment in the catalyst synthesis, *e.g.*, during calcination[103, 104]. On the one hand, a certain interaction of cobalt with commonly used metal oxide supports via metal-support interactions (MSI) is desired to suppress sintering. However, the formation of inactive phases from MSI, such as cobalt silicate (Co_2SiO_4), cobalt alumina ($CoAl_2O_4$), and cobalt titanate (Co_2TiO_4), emerge on supports under hydrothermal conditions and are resistant to reduction, *i.e.*, permanently remove cobalt from the catalytic cycle[91]. These transformations can be difficult to detect and require characterisation techniques, such as X-ray diffraction (XRD) and X-ray

absorption spectroscopy (XAS). Hence, formation of MSCs during FTS remains a major driver to catalyst deactivation as described in several studies[102, 105-107]. Lastly, the combination of elevated temperatures and high concentrations of gaseous water in combination with CO drives sintering of cobalt nanoparticles, *i.e.*, nanoparticle growth via atomic or crystallite migration reducing the total active surface area[108]. Sintering not only lowers activity but can also result in a shift from selective catalytic phases, *e.g.,* hcp-Co, to less active or inactive forms. Effective heat management and reactor design are therefore critical for maintaining catalyst structure and function during extended operation.

The presence of water is also reported to alter the catalyst's activity and selectivity. Several studies report of increased activity of Co-based catalysts in the presence of moderate concentrations of H_2O[100, 109-117], which is also reported for Ru-based FT catalysts[118]. This autocatalytic effect increases the turnover frequency (TOF), the olefin selectivity, and the chain growth probability with increasing partial pressure of water[100, 109, 111-113, 115]. Water has been reported to increase the concentration of monomeric species in turn resulting in a lower methane selectivity and the formation of longer carbon chains[111]. In addition, it has been suggested that water decreases the coverage with inactive surface carbon species, which inhibit the FT reaction[118, 119]. However, the exact origin for the effect of water on selectivity and activity remains unclear[100]. It should be noted that co-feeding high concentrations of water in order to simulate high CO conversion levels in experimental studies has been reported to result in competitive adsorption of water and synthesis gas causing deactivation[120-122], but water should not compete effectively with CO at commercially relevant conversion levels[111].

The support material also plays a decisive role in controlling the dispersion and reducibility of cobalt. Weakly interacting supports such as silica are advantageous in lowering the temperature required for cobalt oxide reduction and enabling high metallic surface area[123]. However, this comes with trade-offs, such as increased susceptibility to sintering and irreversible formation of cobalt silicates[115]. Despite these limitations, cobalt remains one of the

most adaptable and scalable metals for CO hydrogenation, especially when paired with appropriate promoters to fine-tune selectivity and stability.

Aside from the stability and activity, adjusting the selectivity remains the biggest challenge in the FTS. For the production of SAF, high yields of long-chain hydrocarbons are targeted with α values large than 0.9[77, 84]. Aside from adjusting the operation conditions (see Figure 11.11), such as the pressure, the catalyst remains the major driver for boosting chain growth (see Figure 11.14). Here, manganese (Mn) has long been studied as a promoter for Co-based catalysts for the FTS due to its unique electronic and structural effects[37]. In low concentrations, Mn typically distributes over the catalyst including the Co surface as finely dispersed Manganese (II) oxide (MnO) or Manganese (II) ion (Mn^{2+}) species, subtly modifying the electronic environment of active sites[124]. This facilitates CO dissociation and hydrogenation steps, often promoting longer hydrocarbon chain formation and reducing methane selectivity[125]. Consequently, the presence of Mn can shift the product distribution towards more desirable C_{5+} hydrocarbons for the production of SAF.

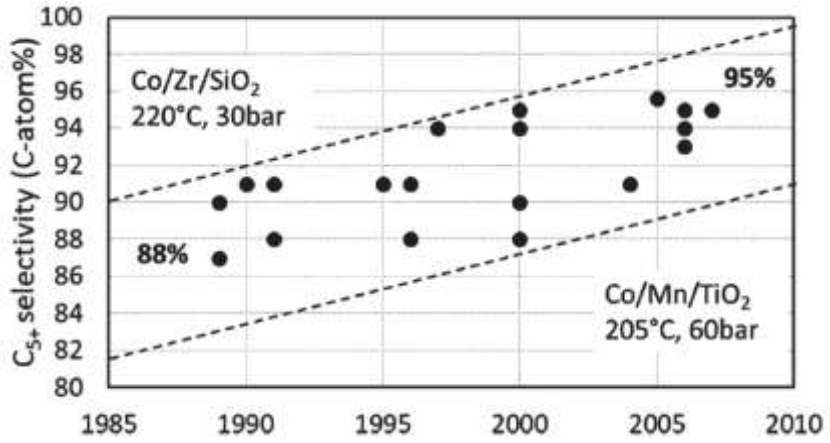

Figure 11.14 *Selectivity of C_{5+} hydrocarbons for individual Shell catalysts based on analysis of patent data.* **Reproduced from ref. 1 with permission from WILEY-VCH, Copyright 2024.**

However, the promotional effects of Mn are highly dependent on its loading. Excessive Mn addition to Co-based catalysts leads to the formation of MnO_x agglomerates or Mn–O–Co

surface phases, which can encapsulate Co particles, reduce accessible active sites, and even hinder Co reduction[126]. This results in diminished activity and a shift in product selectivity toward lighter hydrocarbons or oxygenates. Furthermore, Mn affects the reducibility of Co and thereby demanding increased reduction temperatures during catalyst activation[127]. This delayed reduction can be a double-edged sword as it helps stabilise the Co^0 phase under reaction conditions, but it also makes initial catalyst activation more energy-intensive.

Mn also appears to influence catalyst morphology and stability. By forming spatial or chemical barriers, Mn can inhibit sintering of Co nanoparticles, which enhances the long-term durability of the catalyst under high-pressure and high-temperature conditions[128]. This stabilising role becomes increasingly valuable in CO_2 hydrogenation systems, where thermal gradients and water-rich environments accelerate catalyst deactivation. While Mn does not significantly increase Co dispersion or surface area directly, its modifying effects on the electronic structure and phase of cobalt play a central role in product tuning and catalyst lifetime for efficient SAF production[125].

Despite advances in catalyst formulation, classical catalyst deactivation remains a major challenge during industrial-scale CO hydrogenation and is not limited to aforementioned hydrothermal instability. Deactivation mechanisms are generally categorised as mechanical, thermal, or chemical, each of which can significantly impair catalytic activity and selectivity over time[108]. Mechanically, the accumulation of carbonaceous species, such as coke or polymeric residues, can block access to active sites and obstruct internal pores. These deposits are often formed via Boudouard reaction (Eq. 11.18) or secondary reactions involving heavy hydrocarbon intermediates, particularly under suboptimal H_2:CO ratios or elevated temperatures[129]. Chemical deactivation, meanwhile, often stems from the incorporation of foreign elements that alter the catalyst composition. Sulphur, in particular, is a potent poison, capable of irreversibly binding to cobalt active sites and disrupting the hydrogenation pathway[108]. Although trace amounts of sulphur may exhibit mild promotional effects, consistent exposure results in rapid performance decline. Industrial systems typically employ

guard beds or feed purification to mitigate this risk[88], which become less important when using syngas from clean sources, such as CO_2 and green H_2 via RWGS. Contrary, syngas from gasification requires special care to remove poisons even before adjusting the syngas composition for FTS (see Figure 11.7). Overall, catalyst deactivation represents a mixture of physicochemical processes at various scales, which are influenced by catalyst composition, reaction environment, as well operating conditions and not limited to detrimental effects of high concentrations of water at high conversion levels (see Figure 11.10). A comprehensive understanding of these mechanisms with advanced material design strategies is necessary to extend catalyst lifetimes and ensure consistent performance.

11.4 Selected Recent Milestones for SAF from FTS and Outlook

Multiple pilot and demonstration plants for BTL routes via FTS have been established[48]. BEST Bioenergy and Sustainable Technologies in Austria is significantly advancing the technologies required for BTL and waste-to-liquid routes. A pilot plant with gasification and FTS is operated at the Syngas Platform Vienna in Austria (see Figure 11.7). The gasification infrastructure is a key element of a larger project focused on second-generation biofuel production and improving the economics of sustainable fuel production. NSE Biofuels, a joint venture between Stora Enso Oyj and Neste Oil Corporation, commissioned a BTL plant in Varkaus, Finnland, which is based on gasification of dried forestry residues coupled with FTS. The pilot plant combining biomass drying, a 12 MW gasifier, syngas cleaning, reforming and WGS with FTS with an annual output capacity of 656 t was inaugurated in 2009 and provided the basis for a planned commercial scale process targeting an annual capacity of 100 kt, but the plans were discontinued. In France, the planned BioTFuel plant by Elyse Energy targets a total annual hydrocarbon production capacity of 110 kt with 75 kt of SAF based on gasification of residual biomass and FTS[130].

In 2021, the German company INERATEC started operation of the, at the time, largest PTL plant in Werlte, Germany, converting CO_2 from DAC and mostly biogas with green hydrogen to approx. 350 t fuels per year[131]. A similar pilot plant was commissioned in 2022 in the Port of Hamburg[132]. In 2024, the Swiss company Synhelion inaugurated the first industrial plant for the production of fuels with solar heat as sole energy source in Jülich, Germany. Thermochemical splitting of biogenic CH_4, CO_2, and H_2O is enabled by concentrated solar heat providing process heat at high temperature levels beyond 1000 °C. The produced syngas is then converted in an INERATEC FT stage with subsequent product make-up[133, 134].

Commercial scale was achieved for the PTL route in 2024, when Infinium Electrofuels, USA, commissioned their first production site in Corpus Christi, Texas (production capacity is not communicated). The process is based on captured CO_2 and sustainable H_2, which is converted via RWGS and a modified FTS[135]. In 2025, INERATEC celebrated the inauguration of ERA ONE (see Figure 11.15), a PTL plant in Frankfurt-Höchst (Germany) for the production of fuels and chemicals with special emphasis on the production of SAF. Biogenic CO_2 and green hydrogen are directly sourced within the Frankfurt-Höchst industrial park from a biogas plant and chlorine production, respectively. This feedstock is converted to syngas via RWGS and eventually liquid hydrocarbons via FTS in combination with hydrotreating. The plant is the largest of its kind in Europe with an annual capacity for the production of 2.5 kt of carbon-neutral hydrocarbons. All catalytic reactors are microstructured for optimised heat transfer and material usage. Due to its modular approach, the plant was commissioned in parallel to the construction of the whole capacity[136], which represents another beneficial aspect of scale-up via numbering-up[137]. Recently, several large-scale FT plants for the production of SAF have been announced. Johnson Matthey and bp have licensed their FT technology including FT CANS™ to DG Fuels, which targets an annual production of 600 kt SAF from agricultural waste with production commencing in 2028[138]. Arcadia eFuels, USA, plans to commission several plants combining electrified RWGS with FTS using Topsoe and Sasol technology with

annual plant capacities of 80 kt SAF[139, 140]. Norsk e-Fuel in Norway also announced a series of PTL plants via FTS with CO_2 capture from air or biogenic sources[141].

Figure 11.15 *Era One site by INERATEC representing the largest production plant for e-fuel in Europe. Green hydrogen and CO_2 from biogenic sources are converted into, amongst others, SAF.* ***Source: INERATEC****.*

With respect to the application of synthetic aviation fuels from FT processes, several milestones were achieved in the past decades. However, fossil fuel-based syngas was used in most cases, *i.e.*, no SAF was applied, but technical specifications of the used fuels can also be achieved using sustainable sources due to the feedstock flexibility of the FT process. Since 1998, Sasol has the approval for commercial use of 50% blend of synthetic fuel with conventional jet fuel, the so-called semi-synthetic jet fuel, which is fuelled at the O.R. Tambo international Airport in Johannesburg and was produced via the CtL process[142]. In 2009, a 50% blend of conventional oil-based kerosene with certified synthetic fuel from a GTL process via FTS by Shell was used in the first revenue passenger flight from London to Doha[143]. The next milestone was achieved by the flight from Johannesburg to Cape Town using 100% synthetic

fuel by Sasol in 2010, which was the result of a tedious approval process[142]. With respect to FT-based SAF, the British company Velocys provided a 100% SAF from BTL using wood chips in 2021 for a commercial flight from Tokyo to Sapporo[144].

The absolute quantities of global SAF production, especially via PTL processes, is negligible when compared to the actual demand of aviation fuel. Estimations for an annual production capacity of 5 Mt FT-based SAF in 2030 (see Figure 11.15) represents less than twice the capacity of the natural gas-based Pearl GTL plant. Hence, further scale-up of the production capacity is required to meet the ambitious goals (see Figure 11.1), which comes alongside a scale-down of existing technologies due to decentralisation of sustainable production sites. This is, once again, emphasised by comparison of the capacity of Era One using sustainable feedstock and the Pearl GTL plant in Qatar producing approx. 1000 times more hydrocarbons.

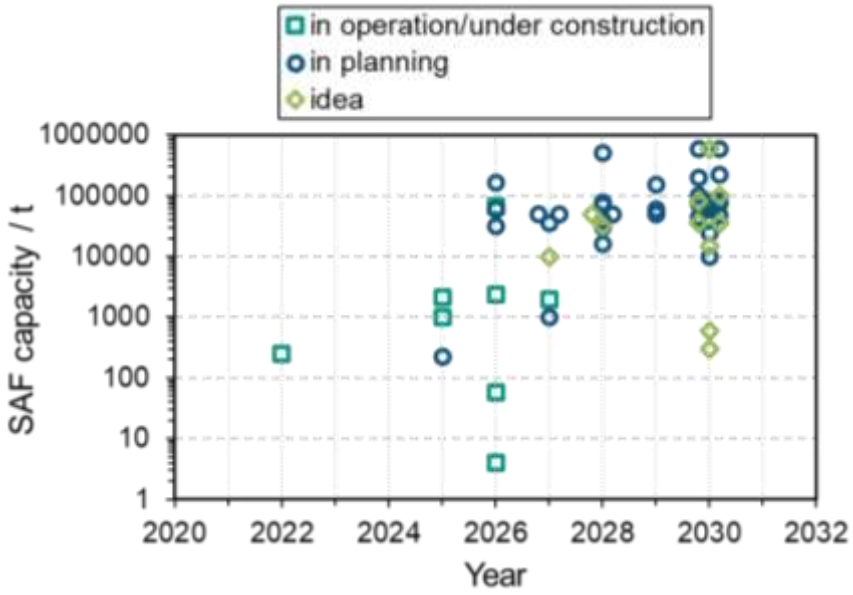

Figure 11.16 *Reported production capacity of SAF for pilot and production sites via FT-based pathways in operation/under construction, in planning, as well as communicated project ideas. The final production target is indicated for (modular) plants commissioned before construction of the full capacity. Data based on SAF monitor by Centre of Competence for Climate, Environment and Noise Protection in Aviation at Hessen Trade & Invest GmbH and NOW GmbH[145].*

ABBREVIATIONS

Al_2O_3	alumina
ASF	Anderson-Schulz-Flory
bpd	barrels per day
BTL	biomass-to-liquid
CALCOR	Industrial Caloric Process
CCLab	Carbon Cycle Lab
CCU	carbon capture utilisation
CFBRs	circulating fluidized beds
CH4	methane
CnHm	hydrocarbons
CO	carbon monoxide
Co	cobalt
Co0	metallic cobalt
CO2	carbon dioxide
Co_2SiO_4	cobalt silicate
Co_2TiO_4	cobalt titanate
Co_3O_4	cobalt (II,III) oxide
$CoAl_2O_4$	cobalt alumina
CoO	cobalt (II) oxide

CORSIA	Carbon Offsetting and Reduction Scheme for International Aviation
COS	carbonyl sulfide
CS_2	carbon disulfide
CTL	coal-to-liquid
DAC	direct air capture
DOC	direct ocean capture
DOE	Department of Energy
DRM	dry reforming of methane
ETS	Emission Trading System
EU	European union
fcc	face-centred cubic
Fe	iron
FFBRs	fixed fluidized beds
FT	Fischer-Tropsch
FT CANS™	compact advanced non-slurry Fischer-Tropsch reactor from JM and bp
FTS	Fischer-Tropsch synthesis
GTL	gas-to-liquid
H:C	hydrogen-to-carbon ratio
H_2	hydrogen
H_2O	steam / water
H_2S	hydrogen sulfide

HCl	hydrochloric acid
HCN	hydrogen cyanide
hcp	hexagonal closed-packed
HEFA	hydropressed esters and fatty acids
HTFTS	high temperature Fischer-Tropsch synthesis
HVO	hydrotreated vegetable oil
ICAO	International Civil Aviation Organisation
In_2O_3	indium(III) oxide
KIT	Karlsruhe Institute of Technology
La_2O_3	lanthana
LTFTS	low temperature Fischer-Tropsch synthesis
Mn	manganese
Mn^{2+}	manganese (II) ion
MnO	manganese (II) oxide
MSCs	metal-support compounds
MSI	metal-support interactions
MTJ	methanol-to-jet fuel
N_2	nitrogen
NH_3	ammonia
O_2	oxygen
PetroSA	Petroleum, Oil and Gas Corporation of South Africa

p_{H2O}/p_{H2}	partial pressure ratio of the product water to the reactant hydrogen
PRC	People's Republic of China
Pt	platinum
PTL	power-to-liquid
Re	rhenium
Rh	rhodium
RSA	Republic of South Africa
Ru	ruthenium
RWGS	reverse water-gas shift
SAF	sustainable aviation fuel
Sasol	South African Coal, Oil and Gas Corporation
SBCRs	slurry-phase bubble column reactors
SiO_2	silica
SMDS	middle distillate synthesis process from Shell
SPRAG	sulphur passivated reforming
SRM	steam reforming of methane
syngas	synthesis gas
Th	thorium
TiO_2	titania
TOF	turnover frequency
TPR	temperature-programmed reduction

USA	United States of America
WGS	water-gas shift
XAS	X-ray absorption spectroscopy
XRD	X-ray diffraction
ZnO	zinc oxide
Zr	zirconium
ZrO_2	zirconia
α	chain-growth probability

ACKNOWLEDGEMENTS

The authors gratefully acknowledge the financial support of the German Federal Ministry of Research, Technology and Space (BMFTR) within the CARE-O-SENE project (03SF0673)[146], that connects German and South African partners for the development of optimized catalyst for producing green kerosene. The goal of the research project is to provide a competitive green alternative for the aviation sector. Further, INERATEC is acknowledged for providing Figure 11.15.

References

1. D. J. Moodley, T. Botha, R. Crous, J. Potgieter, J. Visagie, R. Walmsley and C. Dwyer, *Catalysis for a Sustainable Environment: Reactions, Processes and Applied Technologies*, *Catalysis for Sustainable Aviation Fuels: Focus on Fischer-Tropsch Catalysis*, Wiley, 2024.

2. M. A. Vannice, *J. Catal.*, 1975, **37**, 449.

3. Regulation (EU) 2023/2405 of the European Parliament and of the Council of 18 October 2023 on ensuring a level playing field for sustainable air transport (ReFuelEU Aviation),

press release, EU: Directorate-General for Climate Action, 25.03.2025, https://climate.ec.europa.eu/eu-action/transport/reducing-emissions-aviation_en#:~:text=In%20July%202021%2C%20the%20European,2030%20%2C%20compared%20to%201990%20levels, (accessed 30.07.2025).

4. Pathways to Commercial Liftoff for Sustainable Aviation Fuel, press release, U.S. Department of Energy, 13.11.2024, https://www.energy.gov/articles/us-department-energy-releases-new-report-pathways-commercial-liftoff-sustainable-aviation, (accessed 30.07.2025).

5. M. Hook, D. Fantazzini, A. Angelantoni and S. Snowden, *Phil. Trans. R. Soc. A*, 2014, **372**, 20120319.

6. F. Fischer and H. Tropsch, *Berichte der Dtsch. Chem. Gesellschaft*, 1926, **59**, 830.

7. F. Fischer and H. Tropsch, *Berichte der Dtsch. Chem. Gesellschaft*, 1926, **59**, 832.

8. F. Kainer, *Die Kohlenwasserstoff-Synthese nach Fischer-Tropsch*, Springer, Berlin, 1950.

9. H. Schulz, *Appl. Catal., A*, 1999, **186**, 3.

10. A. P. Steynberg, *Fischer-Tropsch Technology*, *Introduction to Fischer-Tropsch Technology*, Elsevier, Amsterdam, 2004.

11. M. E. Dry, *Catal. Today*, 2002, **71**, 227.

12. M. E. Dry and A. P. Steynberg, *Fischer-Tropsch Technology*, *Commercial FT Process Applications*, Elsevier, Amsterdam, 2004.

13. T. McMahon, Historical Crude Oil Prices (Table), Inflationdata.com, 15.07.2025, https://inflationdata.com/articles/inflation-adjusted-prices/historical-crude-oil-prices-table/, (accessed 30.07.2025).

14. R. Keeling, Scripps CO_2 program, UC San Diego Scripps Institution of Oceangraphy, https://scrippsco2.ucsd.edu/, (accessed 30.07.2025).

15. X. Lan, Trends in atmospheric carbon dioxide (CO_2), NOAA GML, 05.08.2025, https://gml.noaa.gov/ccgg/trends/, (accessed 30.07.2025).

16. O. P. R. van Vliet, A. P. C. Faaij and W. C. Turkenburg, *Energy Convers. Manag.*, 2009, **50**, 855.

17. R. Guettel, U. Kunz and T. Turek, *Chem. Eng. Technol.*, 2008, **31**, 746.

18. BP Statistical Review of World Energy 2017, press release, BP, 2017, https://www.bp.com/content/dam/bp/business-sites/en/global/corporate/pdfs/energy-economics/statistical-review/bp-statistical-review-of-world-energy-2017-full-report.pdf, (accessed 30.07.2025).

19. X. Hao, G. Dong, Y. Yang, Y. Xu and Y. Li, *Chem. Eng. Technol.*, 2007, **30**, 1157.

20. H. Hao, Z. Liu, F. Zhao, J. Du and Y. Chen, *J. Clean. Prod.*, 2017, **141**, 774.

21. D. Stanway, Ningxia coal-to-liquid plant delivers first shipment: paper, Reuters, 29.12.2016, https://www.reuters.com/article/us-china-energy-ctl/ningxia-coal-to-liquid-plant-delivers-first-shipment-paper-idUSKBN14I011/, (accessed 30.07.2025).

22. Significant coal-to-liquid project in production in Ningxia, China Daily Xinhua, 28.12.2016, https://www.chinadaily.com.cn/china/2016-12/28/content_27805385.htm, (accessed 30.07.2025).

23. S. Nigam and D. Singer, *Sustainability in the Air: Innovators Transforming Aviation for a Greener Future*, Legacy launch pad publishing, 2023.

24. E. van Steen and M. Claeys, *Chem. Eng. Technol.*, 2008, **31**, 655.

25. R. Luque, A. R. de la Osa, J. M. Campelo, A. A. Romero, J. L. Valverde and P. Sanchez, *Energy Environ. Sci.*, 2012, **5**, 5186.

26. M. Perez and R. Perez, *Sol. Energy Adv.*, 2022, **2**.

27. B. M. Weckhuysen and E. T. C. Vogt, *Nature*, 2024, **629**, 295.

28. E. Hanson, C. Nwakile and V. O. Hammed, *Results Surf. Interfaces*, 2025, **18**.

29. A. Majeed, N. Hemmerling and B. J. M. Etzold, *Electrochim. Acta*, 2025, **510**.

30. S. T. Wismann, K.-E. Larsen and P. M. Mortensen, *Angew. Chem. Int. Ed.*, 2021, **61**.

31. C. H. Lin, C. Wan, Z. Ru, C. Cremers, P. Mohapatra, D. L. Mantle, K. Tamakuwala, A. B. Höfelmann, M. W. Kanan, J. Rivas-Davila and J. A. Fan, *Joule*, 2024, **8**, 2938.

32. E. Turan, R. Dieckmann, M. Geske, R. N. d'Alnoncourt, M. Bender, J. Bode, B. Frank, D. Zakgeym, G. Kolios and F. Rosowski, *Chem. Eng. J.*, 2025, **514**.

33. D. Maporti, S. Guffanti, F. Galli, P. Mocellin and G. Pauletto, *Chem. Eng. J.*, 2024, **499**.

34. BASF, SABIC, and Linde celebrate the start-up of the world's first large-scale electrically heated steam cracking furnace, press release, BASF, 17.04.2024, https://www.basf.com/global/en/media/news-releases/2024/04/p-24-177, (accessed 22.08.2025).

35. EReTech Pilot 1 is onfield! , press release, EReTech, 01.07.2024, https://www.eretech.eu/eretech-pilot-1-is-onfield/, (accessed 22.08.2025).

36. B. E. Rogachuk and J. A. Okolie, *Energy Convers. Manage.*, 2024, **302**.

37. T. Kaneko, F. Derbyshire, E. Makino, D. Gray, M. Tamura and K. Li, *Ullmann's Encyclopedia of Industrial Chemistry*, *Coal Liquefaction*, Wiley-VCH, 2001.

38. C. Higman, *Combustion Engineering Issues for Solid Fuel Systems*, *Gasification*, Academic Press, 2008.

39. C. Higman and M. van der Burgt, *Gasification*, *The Kinetics of Gasification and Reactor Theory*, Gulf Professional Publishing, 2, 2008.

40. Y. Tian, Z. Luo, D. He, Y. Yang, S. Liang, W. Liu and L. Yuan, *Biomass Convers. Biorefin.*, 2022, **14**.

41. E. Henrich, N. Dahmen and E. Dinjus, *Biofuels, Bioprod. Bioref.*, 2009, **3**, 28.

42. N. Dahmen, J. Abeln, M. Eberhard, T. Kolb, H. Leibold, J. Sauer, D. Stapf and B. Zimmerlin, *WIREs Energy Environ.*, 2017, **6**.

43. M. Eberhard, U. Santo, B. Michelfelder, A. Guenther, P. Weigand, J. Matthes, P. Waibel, eyer Hagen, V. and T. Kolb, *ChemBioEng Rev.*, 2020, **7**, 106.

44. Carbon Cycle Lab: From Waste to Industrial Raw Materials, press release, KIT, 04.03.2025, https://www.kit.edu/kit/english/pi_2025_013_carbon-cycle-lab-from-waste-to-industrial-raw-materials.php, (accessed 30.07.2025).

45. A. Lappas and E. Heracleous, *Handbook of Biofuels Production*, *18 - Production of biofuels via Fischer–Tropsch synthesis: Biomass-to-liquids*, Woodhead Publishing, 2016.

46. J. R. C. Rey, A. Longo, B. Rijo, C. M. Pedrero, L. A. C. Tarelho, P. S. D. Brito and C. Nobre, *Fuel*, 2024, **377**.

47. C. N. Hamelinck, A. P. C. Faaij, H. den Uil and H. Boerrigter, *Energy*, 2004, **29**, 1743.

48. R. Rauch, J. Hrbek and H. Hofbauer, *WIREs Energy Environ.*, 2013, **3**, 343.

49. K. Chouhan, S. Sinha, S. Kumar and S. Kumar, *Int. J. Hydrogen Energy*, 2021, **46**, 26809.

50. R. Bove and P. Lunghi, *Energy Convers. Manage.*, 2006, **47**, 1391.

51. K. Wittich, M. Kraemer, N. Bottke and S. Schunk, *ChemCatChem*, 2020, **12**, 2130.

52. N. A. K. Aramouni, J. G. Touma, B. A. Tarboush, J. Zeaiter and M. N. Ahmad, *Renew. Sustain. Energy Rev.*, 2018, **82**, 2570.

53. Y. Wang, L. Yao, Y. Wang, S. Wang, Q. Zhao, D. Mao and C. Hu, *ACS Catal.*, 2018, **8**, 6495.

54. S. T. Oyama, P. Hacarlioglu, Y. Gu and D. Lee, *Int. J. Hydrogen Energy*, 2012, **37**, 10444.

55. Y. T. Shah, *Water for Energy and Fuel Production*, Taylor & Francis, 2014.

56. H. Er-rbib, C. Bouallou and F. Werkoff, *Energy Procedia*, 2012, **29**, 156.

57. E. Rezaei and S. Dzuryk, *Chem. Eng. Res. Des.*, 2019, **144**, 354.

58. ST. C. Teuner, P. Neumann and F. von Linde, *Oil Gas Eur. Mag.*, 2001, **3**.

59. A. Milanov, E. Schwab and A. Schaefer, inventors; BASF SE, assignee. Catalyst composition for the steam reforming of methane in fuel cells. USA patent 8993477. 2012 31.03.2015.

60. M. L. T. Triviño, N. C. Arriola Jr., Y. S. Kang and J. G. Seo, *Chem. Eng. J.*, 2024, **487**.

61. Y. Daza and J. Kuhn, *RSC Adv.*, 2016, **6**, 49675.

62. D. Álvarez-Hernández, M. Marín-Sánchez, L. Lobo-Andrades, L. Azancot, L. F. Bobadilla, S. Ivanova and M. A. Centeno, *Catal. Today*, 2023, **422**.

63. W. Marquart, S. Raseale, G. Prieto, A. Zimina, B. B. Sarma, J.-D. Grunwaldt, M. Claeys and N. Fischer, *ACS Catal.*, 2021, **11**, 1624.

64. L. P. Dancuart, R. de Haan and A. de Klerk, *Fischer-Tropsch Technology*, *Processing of Primary Fischer-Tropsch Products*, Elsevier, Amsterdam, 2004.

65. A. P. Steynberg, M. E. Dry, B. H. Davis and B. B. Breman, *Fischer-Tropsch Technology*, *Fischer-Tropsch Reactors*, Elsevier, Amsterdam, 2004.

66. T. N. Eran, J. Guyot, D. C. Boffito and G. S. Patience, *Chem. Eng. J.*, 2024, **500**.

67. J. Lefebvre, S. Bajohr and T. Kolb, *Renew. Energy*, 2020, **151**, 118.

68. J. Eilers, S. A. Posthuma and S. T. Sie, *Catal. Lett.*, 1990, **7**, 253.

69. M. Loewert and P. Pfeifer, *ChemEngineering*, 2020, **4**, 21.

70. M. Peacock, J. Paterson, L. Reed, L. Davies, S. Carter, A. Coe and J. Clarkson, *Top Catal.*, 2020, **63**, 328.

71. A. P. Steynberg, S. R. Deshmukh and H. J. Robota, *Catal. Today*, 2018, **299**, 10.

72. D. R. Palo, V. S. Stenkamp, R. A. Dagle and G. N. Jovanovic, *Micro Process Engineering: Fundamentals, Devices, Fabrication, and Applications*, *Industrial Applications of Microchannel Process Technology in the United States*, Wiley-VCH, Weinheim, 2013.

73. M. Loewert, J. Hoffmann, P. Piermartini, M. Selinsek, R. Dittmeyer and P. Pfeifer, *Chem. Eng. Technol.*, 2019, **42**, 1.

74. E. van Steen, M. Claeys, M. E. Dry, J. van de Loosdrecht, E. L. Viljoen and J. L. Visagie, *J. Phys. Chem. B*, 2005, **109**, 3575.

75. Lj. Gavrilović, S. S. Kazi, A. Oliveira, O. L. I. Encinas and E. A. Blekkan, *Catal. Today*, 2024, **432**.

76. D. Liuzzi, E. Fernandez, S. Perez, E. Ipiñazar, A. Arteche, J. Fierro, J. Viviente, D. Pacheco Tanaka and S. Rojas, *Rev. Chem. Eng.*, 2022, **38**, 55.

77. A. de Klerk, Wiley-VCH, Weinheim, 2011.

78. J. van de Loosdrecht, F. G. Botes, I. M. Ciobica, A. Ferreira, P. Gibson, D. J. Moodley, A. M. Saib, J. L. Visagie, C. J. Weststrate and J. W. Niemantsverdriet, *Comprehensive Inorganic Chemistry II: From Elements to Applications*, *Fischer-Tropsch Synthesis: Catalysts and Chemistry*, Elsevier, Oxford, 2, 2013.

79. M. E. Dry, *Catalysis*, *Chapter 4 The Fischer-Tropsch Synthesis*, De Gruyter, Berlin, Boston, 1982.

80. C. D. Frohning, H. H. Kölbel, M. Ralek, W. Rottig, F. Schnur and H. Schulz, *Chemierohstoffe aus Kohle*, Thieme, 1977.

81. L. Brübach, M. Wolf and P. Pfeifer, *Powerfuels: Status and Prospects*, *Fischer-Tropsch Synthesis*, Springer, 2025.

82. G. P. van der Laan and A. A. C. M. Beenackers, *Catal. Rev. Sci. Eng.*, 1999, **41**, 255.

83. H. Schulz, G. Schaub, M. Claeys and T. Riedel, *Appl. Catal., A*, 1999, **186**, 215.

84. S. Bube, N. Bullerdiek, S. Voß and M. Kaltschmitt, *Fuel*, 2024, **366**.

85. CARE-O-SENE achieves milestone in the commercialisation of sustainable aviation fuels, press release, CARE-O-SENE, 01.10.2024, https://care-o-sene.com/en/2024/10/02/care-o-sene-erreicht-meilenstein-zur-kommerzialisierung-nachhaltiger-flugkraftstoffe/, (accessed 30.07.2025).

86. D. Vervloet, F. Kapteijn, J. Nijenhuisa and J. R. van Ommena, *Catal. Sci. Technol.*, 2012, **2**, 1221.

87. C. L. Tucker, M. Claeys and E. van Steen, *Catal. Sci. Technol.*, 2020, **10**, 7056.

88. M. E. Dry, *Handbook of Heterogeneous Catalysis*, *The Fischer–Tropsch (FT) Synthesis Processes*, 2008.

89. P.J. van Berge and R.C. Everson, *Stud. Surf. Sci. Catal.*, 1997, **107**, 207.

90. R.B. Anderson, *Hydrocarbon Synthesis, Hydrogenation and Cyclization*, *Catalysts for the Fischer-Tropsch synthesis*, Reinhold, 1956.

91. M. Wolf, F. Fischer and M. Claeys, *Chem Catal.*, 2021, **1**, 1014.

92. M. Wolf, H. Kotzé, N. Fischer and M. Claeys, *Faraday Discuss.*, 2017, **197**, 243.

93. M. Wolf, E. K. Gibson, E. J. Olivier, J. H. Neethling, C. R. A. Catlow, N. Fischer and M. Claeys, *Catal. Today*, 2020, **342**, 71.

94. M. E. Dry, *Fischer-Tropsch Technology*, *FT catalysts*, Elsevier, Amsterdam, 2004.

95. W. T. Ralston, G. Melaet, T. Saephan and G. A. Somorjai, *Angew. Chemie - Int. Ed.*, 2017, **56**, 7415.

96. A. Tuxen, S. Carenco, M. Chintapalli, C. H. Chuang, C. Escudero, E. Pach, P. Jiang, F. Borondics, B. Beberwyck, A. P. Alivisatos, G. Thornton, W. F. Pong, J. Guo, R. Perez, F. Besenbacher and M. Salmeron, *J. Am. Chem. Soc.*, 2013, **135**, 2273.

97. P. van Helden, I. M. Ciobîcă and R. L. J. Coetzer, *Catal. Today*, 2016, **261**, 48.

98. G. L. Bezemer, J. H. Bitter, H. P. C. E. Kuipers, H. Oosterbeek, J. E. Holewijn, X. Xu, F. Kapteijn, A. J. van Dillen and K. P. de Jong, *J. Am. Chem. Soc.*, 2006, **128**, 3956.

99. I. C. ten Have and B. M. Weckhuysen, *Chem Catal.*, 2021, **1**, 339.

100. E. Iglesia, *Appl. Catal., A*, 1997, **161**, 59.

101. M. Wolf, F. Fischer and M. Claeys, *Nat. Catal.*, 2020, **3**, 962.

102. N. E. Tsakoumis, J. C. Walmsley, M. Rønning, W. van Beek, E. Rytter and A. Holmen, *J. Am. Chem. Soc.*, 2017, **139**, 3706.

103. W. Chu, P. A. Chernavskii, L. Gengembre, G. A. Pankina, P. Fongarland and A. Y. Khodakov, *J. Catal.*, 2007, **252**, 215.

104. N. E. Tsakoumis, R. E. Johnsen, W. van Beek, M. Rønning, E. Rytter and A. Holmen, *Chem. Comm.*, 2016, **52**, 3239.

105. S. Storsæter, Ø. Borg, E. A. Blekkan, B. Tøtdal and A. Holmen, *Catal. Today*, 2005, **100**, 343.

106. M. Wolf, E. K. Gibson, E. J. Olivier, J. H. Neethling, C. R. A. Catlow, N. Fischer and M. Claeys, *ACS Catal.*, 2019, **9**, 4902.

107. J. G. Moya-Cancino, A. P. Honkanen, A. M. J. van der Eerden, H. Schaink, L. Folkertsma, M. Ghiasi, A. Longo, F. M. F. de Groot, F. Meirer, S. Huotari and B. M. Weckhuysen, *ChemCatChem*, 2019, **11**, 1.

108. N. E. Tsakoumis, M. Rønning, Ø. Borg, E. Rytter and A. Holmen, *Catal. Today*, 2010, **154**, 162.

109. N. Fischer, B. Clapham, T. Feltes and M. Claeys, *ACS Catal.*, 2015, **5**, 113.

110. A. M. Hilmen, D. Schanke, K. F. Hanssen and A. Holmen, *Appl. Catal., A*, 1999, **186**, 169.

111. C. J. Bertole, C. A. Mims and G. Kiss, *J. Catal.*, 2002, **210**, 84.

112. S. Krishnamoorthy, M. Tu, M. P. Ojeda, D. Pinna and E. Iglesia, *J. Catal.*, 2002, **211**, 422.

113. M. Lualdi, S. Lögdberg, M. Boutonnet and S. Järås, *Catal. Today*, 2013, **214**, 25.

114. S. Lögdberg, M. Boutonnet, J. C. Walmsley, S. Järås, A. Holmen and E. A. Blekkan, *Appl. Catal., A*, 2011, **393**, 109.

115. J. Li, G. Jacobs, T. Das, Y. Zhang and B. Davis, *Appl. Catal., A*, 2002, **236**, 67.

116. T. K. Das, W. A. Conner, J. Li, G. Jacobs, M. E. Dry and B. H. Davis, *Energy Fuels*, 2005, **19**, 1430.

117. H. Schulz, M. Claeys and S. Harms, *Natural Gas Conversion IV*, *Effect of water partial pressure on steady state Fischer-Tropsch activity and selectivity of a promoted cobalt catalyst*, Elsevier, Amsterdam, 1997.

118. M. Claeys and E. van Steen, *Catal. Today*, 2002, **71**, 419.

119. A. M. Saib, D. J. Moodley, I. M. Ciobîcă, M. M. Hauman, B. H. Sigwebela, C. J. Weststrate, J. W. Niemantsverdriet and J. van de Loosdrecht, *Catal. Today*, 2010, **154**, 271.

120. E. Rytter and A. Holmen, *ACS Catal.*, 2017, **7**, 5321.

121. J. Li, X. Zhan, Y. Zhang, G. Jacobs, T. Das and B. H. Davis, *Appl. Catal., A*, 2002, **228**, 203.

122. A. K. Dalai and B. H. Davis, *Appl. Catal., A*, 2008, **348**, 1.

123. S. Storsæter, B. Tøtdal, J. C. Walmsley, B. S. Tanem and A. Holmen, *J. Catal.*, 2005, **236**, 139.

124. G. Jacobs, T. K. Das, Y. Zhang, J. Li, G. Racoillet and B. H. Davis, *Appl. Catal., A*, 2002, **233**, 263.

125. C. L. Tucker, Y. Ragoo, S. Mathe, L. Macheli, A. Bordoloi, T. C. R. Rocha, S. Govender, P. J. Kooyman and E. van Steen, *J. Catal.*, 2022, **411**, 97.

126. N. Thibanyane, J. Gorimbo and Y Yao, *Reactions*, 2024, **5**, 607.

127. E. van Steen, G. S. Sewell, R. A. Makhothe, C. Micklethwalte, H. Manstein, M. de Lange and O'Connor C. T., *J. Catal.*, 1996, **162**, 220.

128. L. M. van Koppen, A. Iulian Dugulan, G. Leendert Bezemer and E. J. M. Hensen, *J. Catal.*, 2023, **428**, 115173.

129. C. H. Bartholomew, *Appl. Catal.*, 2001, **212**, 17.

130. Elyse Energy, Avril, Axens, Bionext and IFP Energies nouvelles announce the creation of the BioTJet plant in the Lacq industrial area, a new centre of excellence for sustainable fuels, press release, Elyse, 23.06.2023, https://elyse.energy/en/elyse-energy-avril-axens-bionext-and-ifp-energies-nouvelles-announce-the-creation-of-the-biotjet-plant-in-the-lacq-industrial-area-a-new-centre-of-excellence-for-sustainable-fuels, (accessed 30.07.2025).

131. First industrial power-to-liquid pilot plant, press release, INERATEC, 2025, https://www.ineratec.de/de/news/erste-industrielle-power-liquid-pilotanlage (accessed 30.07.2025).

132. Commissioning starts in Hamburg, press release, INERATEC, 30.07.2025, https://www.ineratec.de/en/news/plant-commissioning-hamburg-started, (accessed 30.07.2025).

133. Synhelion inaugurates DAWN – the world's first industrial plant for the production of solar fuels, press release, Synhelion, 20.06.2024, https://synhelion.com/news/synhelion-inaugurates-dawn, (accessed 30.07.2025).

134. D. Marxer, P. Furler, J. Scheffe, H. Geerlings, C Falter, V. Batteiger, A Sizmann and A. Steinfeld, *Energy Fuels*, 2015, **29**, 3241.

135. Infinium's Project Pathfinder is World's First Fully Operational eFuels Facility, PR Newswire, 21.03.2024, https://www.prnewswire.com/news-releases/infiniums-project-pathfinder-is-worlds-first-fully-operational-efuels-facility-302095002.html, (accessed 30.07.2025).

136. INERATEC opens ERA ONE: Europe's largest e-Fuel production plant goes into operation in Frankfurt, press release, INERATEC, https://www.ineratec.de/en/news/ineratec-opens-era-one-europes-largest-e-fuel-production-plant-goes-operation-frankfurt, (accessed 30.07.2025).

137. Y. Ganjkhanlou, E. Boymans and B. Vreugdenhil, *Fuels*, 2025, **6**.

138. DG Fuels, Johnson Matthey & bp Partner for Largest Fischer-Tropsch SAF Plant, press release, DG Fuels, 10.04.2024, https://dgfuels.com/2024/04/10/dg-fuels-johnson-matthey-bp-partner-for-largest-fischer-tropsch-saf-plant/ (accessed 30.07.2025).

139. Arcadia eFuels Awarded $14.6 Million for Project ARC in Texas, press release, Arcadia, 16.08.2024, https://arcadiaefuels.com/arcadia-efuels-awarded-14-6-million-for-project-arc-in-texas/ (accessed 30.07.2025).

140. First commercial eFuels-for-aviation plant in Denmark on schedule for 2026 – Arcadia selects Topsoe and Sasol technology, press release, Sasol, 10.05.2023, https://www.sasol.com/media-centre/media-releases/first-commercial-efuels-aviation-plant-denmark-schedule-2026-arcadia-selects-topsoe-and-sasol, (accessed 30.07.2025).

141. Projects Scaling production to make aviation sustainable, press release, Norsk E-Fuel, 2025, https://www.norsk-e-fuel.com/projects, (accessed 30.07.2025).

142. Sasol takes to the skies with the world's first fully synthetic jet fuel, Sasol, 22.09.2010, https://www.sasol.com/sasol-takes-skies-worlds-first-fully-synthetic-jet-fuel (accessed 30.07.2025).

143. Paving the way for Sustainable Aviation Fuels, Shell, 2025, https://www.shell.com/business-customers/aviation/100years/flying-together/paving-saf.html, (accessed 30.07.2025).

144. Velocys technology powers first commercial flight, press release, Velocys, 21.06.2021, https://velocys.com/2021/06/21/velocys-technology-powers-first-commercial-flight/ (accessed 30.07.2025).

145. SAF-Monitor, Cena Hessen, https://www.cena-hessen.de/en/projects/saf-monitor/, (accessed 30.07.2025).

146. CARE-O-SENE: Research for a green future: CARE-O-SENE – Catalyst Research for Sustainable Kerosene, CARE-O-SENE, https://care-o-sene.com/en/, (accessed 30.07.2025).